

clones, according to the teratoma-forming activity of the iPS-derived neurospheres after transplantation into the NOD/SCID mouse brain.

Here, we first performed a detailed examination of the neural differentiation potential of a safe iPS clone, 38C2, which was established from mouse embryonic fibroblasts (MEFs) by the introduction of four factors, including *c-Myc*, and by the selection for *Nanog* expression (19, 28), and compared them with mouse ES cells (EB3) (29, 30). 38C2 iPS cells and EB3 ES cells were induced into embryoid bodies (EBs) in medium containing a low concentration of retinoic acid, then dissociated and cultured in suspension in serum-free medium with FGF-2 for 7 or 8 d to form primary neurospheres (PNS) (38C2 iPS/EB3 ES-PNS) (29). These PNSs were dissociated and formed secondary neurospheres (38C2 iPS/EB3 ES-SNS) under the same conditions (Fig. 1A). To induce further differentiation, 38C2 iPS-SNSs were adherently cultured in the absence of FGF-2, resulting in the generation of *Tuj1*⁺ neurons (4.9 ± 0.8%), *GFAP*⁺ astrocytes (11.3 ± 1.2%), and *CNPase*⁺ oligodendrocytes (3.7 ± 0.9%), as well as *Nestin*⁺ neural progenitor cells (25.9 ± 6.5%; Fig. 1B and C), suggesting that 38C2 iPS-SNS have similar differentiation potentials to EB3 ES-SNS. The 38C2 iPS-SNSs could also generate *TH*⁺ catecholaminergic, *5HT*⁺ serotonergic, and *GAD67*⁺ GABAergic neurons (Fig. S1). RT-PCR analysis of the expression of cell-type-specific markers in the progeny of the 38C2 iPS cells showed drastic decrease of the expression of undifferentiated ES cell marker genes, such as *Nanog*, *Eras*, and *Oct3/4*, and the up-regulation of neural markers such as *Sox1*, *βIII-tubulin*, and *GFAP* during the neural differentiation of 38C2 iPS cells, similar to EB3 ES cells (Fig. 1D).

Moreover, electrophysiological analysis using whole-cell patch clamping in both the 38C2 iPS-PNS- and EB3 ES-PNS-derived neurons after 21–28 d of adherent differentiation showed tetrodotoxin (TTX; 1 μM)-sensitive repetitive action potentials in the current-clamp mode [38C2 iPS-PNS (*n* = 11 of 16) and EB3 ES-PNS (*n* = 5 of 7)] (Fig. S2A) and very rapid inward currents immediately followed by transient outward currents in voltage-clamp mode (Fig. S2B 1 and 2). Steady outward currents, similar to those mediated by delayed-rectifier *K*⁺ channels, were also observed (Fig. S2B 1 and 2). These findings suggest that 38C2 iPS-PNSs produced neuronal cells equipped with functional channels that could generate and modify action potentials (SI Text).

Safe MEF-iPS Cells Can Differentiate into Trilineage Neural Cells in the Injured Spinal Cord Without Tumorigenesis.

Previously, we con-

firmed that SNSs from the safe 38C2 MEF-iPS cell clone survived and showed no teratoma-forming activity in the NOD/SCID mouse brain for 24 wk after transplantation (27) (Fig. S3). 38C2 iPS-SNSs that were transplanted into the intact spinal cord survived and differentiated into trilineage neural cells without any tumorigenesis (Fig. S4). Next, to evaluate their therapeutic effects in the mouse SCI model, we transplanted 38C2 iPS-SNSs into the contused spinal cord 9 d after injury and compared them with EB3 ES-SNSs, using adult fibroblasts and PBS as controls. We also made a comparison with 38C2 iPS-PNSs, because we recently confirmed that the transplantation of ES cell-derived SNSs, but not PNSs, provides therapeutic benefit after SCI (31). We transplanted 38C2 iPS-SNSs that had been prelabeled by lentivirus to express both *CBR1uc* and *mRFP* (32, 33) into the lesion epicenter 9 d after the injury. Bioluminescence imaging (BLI) analysis (34), which detects luciferase photon signals only from living cells, revealed an approximate graft survival rate of 18% at 35 d after transplantation (Fig. 2A). We also histologically confirmed that the grafted cells survived and exhibited no apparent evidence of tumorigenesis (Fig. 2B), and that there were no *Nanog*⁺ cells (Fig. S5), at least during our observation

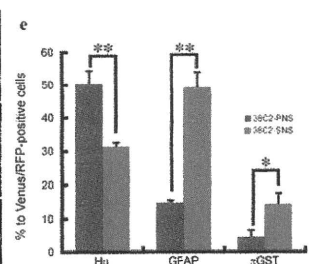
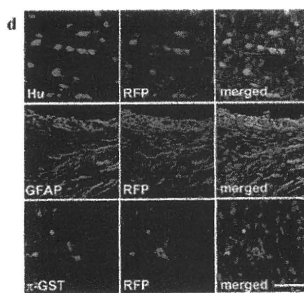
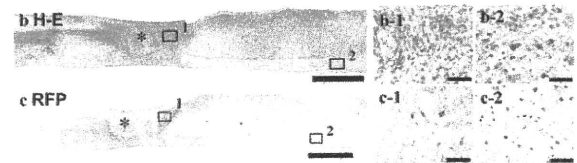
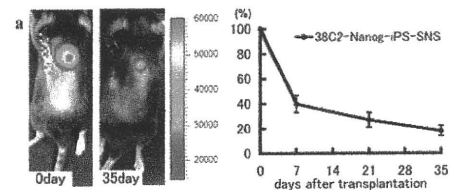


Fig. 2. Transplanted SNSs derived from safe MEF-iPS clones survive without any evidence of tumorigenesis and differentiate into trilineage neural cells in the injured spinal cord. (A) Representative BLI images of a mouse in which *CBR1uc*-expressing 38C2 iPS-SNSs were transplanted into the injured spinal cord (Left, immediately after transplantation; Right, 42 d after transplantation). Quantification of the photon intensity revealed that ~60% of the grafted cells were lost within 7 d after transplantation, and ~20% of the cells survived 35 d after transplantation. Values are means ± SEM (*n* = 6). (B) H&E and (C) anti-RFP DAB staining of sagittal sections of the spinal cord 42 d after injury (38C2 iPS-SNS transplanted). There was no evidence of tumorigenesis (B). No significant nuclear atypia was observed in magnified images of the boxed areas showing the lesion epicenter (B-1) or white matter caudal to the transplantation site (B-2). Grafted cells survived and were diffusely distributed rostral and caudal to the lesion site (C). Higher-magnification images of the boxed areas showing the lesion site (C-1) and white matter caudal to the lesion site (C-2). *Lesion epicenter. (D) Immunohistochemical analyses of 38C2 iPS-SNSs grafted into spinal cord 42 d after injury, revealing grafted cells double-positive for RFP and markers of neural lineages. (E) Quantitative analyses of *Hu*⁺ neurons, *GFAP*⁺ astrocytes, and π -*GST*⁺ oligodendrocytes. Values are means ± SEM (*n* = 3 each; **P* < 0.05, ***P* < 0.01).

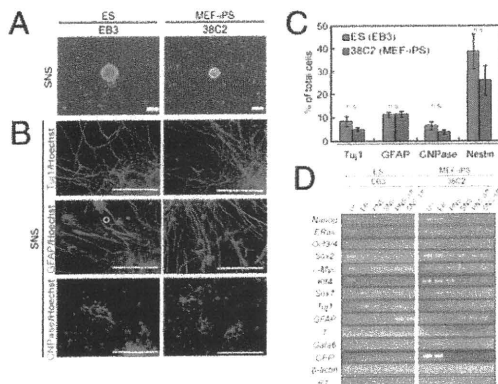


Fig. 1. Neural differentiation of pre-evaluated safe MEF-iPS cells in vitro. (A) Neurospheres derived from EB3 ES cells and 38C2 iPS cells. (Scale bar: 200 μm.) (B) Immunocytochemical analysis of neural cell marker proteins in the differentiated SNSs derived from EB3 ES and 38C2 iPS cells. (Scale bar: 100 μm.) (C) Neural differentiation efficiencies of neurospheres derived from EB3 ES and 38C2 iPS cells. (*n* = 5, n.s.). (D) RT-PCR analysis of undifferentiated cells (Un.), EBs, PNSs, SNSs, differentiated PNSs (PNS diff.), and SNSs (SNS diff.) of the EB3-ES and 38C2 iPS cells.

period. Grafted RFP⁺ cells were located mainly around the lesion epicenter, whereas some cells had migrated as far as 4 mm rostral and caudal to the graft site (Fig. 2C). In the injured spinal cord, the grafted 38C2 iPS-SNSs differentiated into three types of neural cells, including Hu⁺ neurons (31.4 ± 1.1%), GFAP⁺ astrocytes (49.3 ± 4.5%), and π -GST⁺ oligodendrocytes (14.4 ± 3.0%), whereas 38C2 iPS-PNSs differentiated dominantly into neurons—that is, Hu⁺ neurons (50.4 ± 3.8%), GFAP⁺ astrocytes (14.9 ± 0.6%), and π -GST⁺ oligodendrocytes (4.6 ± 1.8%) (Fig. 2D and E and Fig. S6).

Transplantation of SNSs Derived from Safe MEF-iPS Cells into the Injured Spinal Cord Promotes Functional Recovery. The contusive SCI initially caused complete paralysis, followed by gradual recovery that reached a plateau. There were statistically significant differences in Basso mouse scale (BMS) between the 38C2 iPS-SNS and PBS groups at 21, 28, 35, and 42 d after injury, whereas no significant difference was observed between the 38C2 iPS-SNS and EB3 ES-SNS groups. Forty-two days after injury, the 38C2 iPS-SNS-grafted animals could lift their trunks and had significantly better BMS than the PBS control or adult fibroblast-treated animals, which were unable to support their body weight with their hindlimbs (Fig. 3A). To reveal the potential mechanism of functional recovery after 38C2 iPS-SNS transplantation, we conducted further histological analyses. By Luxol Fast Blue (LFB) staining, 38C2 iPS-SNS-grafted mice showed a significantly larger myelinated area at the lesion epicenter than the PBS control mice at 42 d after injury (Fig. 3B). We also found that grafted 38C2 iPS-SNS-derived cells myelinated NF200⁺ host neuronal fibers, confirmed by the positive staining of RFP and myelin basic protein (MBP; Fig. 3C), indicating that graft cell-derived oligodendrocytes were capable of remyelination. For further confirmation of the myelinat-

ing ability of 38C2 iPS-SNSs, we transplanted 38C2 iPS-SNSs into the injured spinal cord of MBP-null *shiverer* mice, a severely hypo- and dysmyelinating mutant mouse that lacks the major dense line of CNS myelin (35). Myelinating potential of the grafted 38C2 iPS-SNS-derived cells was confirmed, exhibiting MBP⁺ deposits (Fig. 3D) and the major dense line, by electron microscopic analysis (Fig. 3E).

To determine the effect of the grafted 38C2 iPS-SNSs on serotonergic nerve fibers, which are important for the motor functional recovery of hind limbs (36, 37), we immunostained for 5HT and quantified the positive area at the distal cord 1, 2, and 6 wk after injury. Some of the nerve fibers associated with graft cell-derived Hu⁺ neurons were identified as 5HT⁺ serotonergic fibers, and were prominent at the distal cord compared with the PBS control group (Fig. 4A–C). Quantitative analysis of the serotonergic innervation of the distal cord revealed a significant difference between the 38C2 iPS-SNS and PBS control groups (Fig. 4B). The contusive injury (60 kDyn) resulted in a significant decrease in the number of 5HT⁺ fibers at the distal cord, followed by a slight recovery, which is the nature of contusive SCI. The injection of PBS in the PBS control group did not induce any additional increase in the number of 5HT⁺ fibers at the distal cord. In contrast, innervation of the distal cord by these 5HT⁺ fibers was enhanced by the grafted 38C2 iPS-SNS 6 wk after SCI (Fig. 4B). Moreover, 38C2 iPS-SNS-derived astrocytes, which exhibited a bipolar morphology with long processes, were observed closely associated with the 5HT⁺ serotonergic fibers (Fig. 4D).

Transplantation of Neurospheres Derived from Pre-Evaluated Safe or Unsafe TTF-iPS Cells into the Injured Spinal Cord. Toward the goal of clinical application, we next examined the therapeutic potential

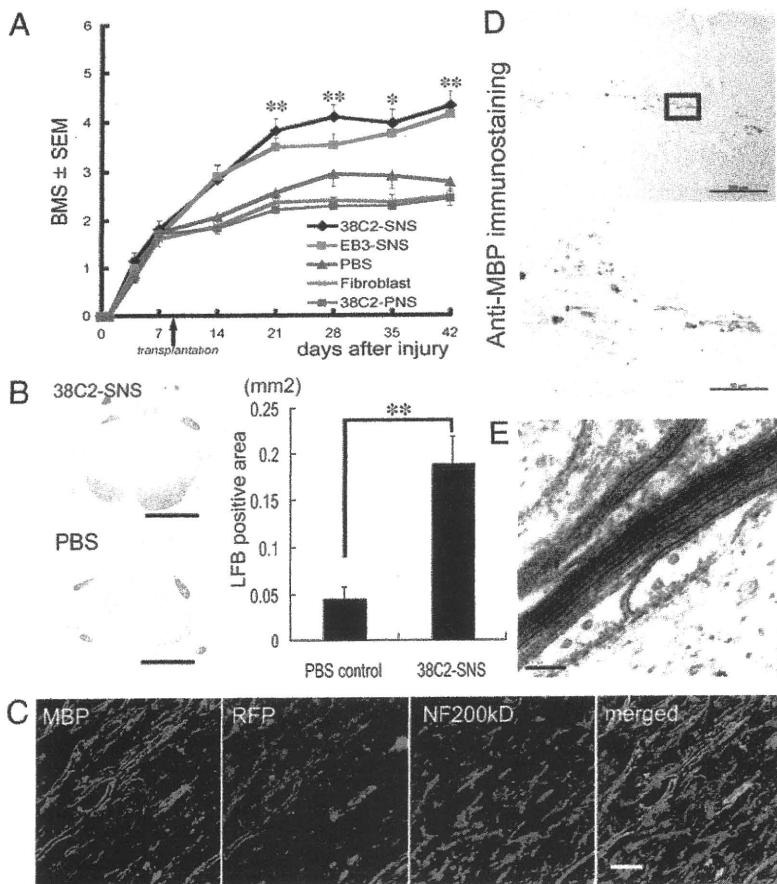


Fig. 3. SNS derived from a safe MEF-iPS clone differentiate into mature oligodendrocytes and promote remyelination. (A) Time course of functional recovery of hind limbs evaluated by BMS. 38C2 iPS-SNS, $n = 19$; EB3 ES-SNS, $n = 15$; PBS, $n = 12$; adult fibroblasts, $n = 13$; 38C2 iPS-PNS, $n = 13$. * $P < 0.05$, ** $P < 0.01$. (B) LFB staining of axial sections of the spinal cord at the lesion epicenter 42 d after injury; 38C2 iPS-SNS-transplanted (Upper Left) and PBS control (Lower Left) animals. Quantification of LFB-positive areas at the lesion epicenter 42 d after injury (Right, $n = 7$ each; ** $P < 0.01$). (C) Immunohistochemistry of 38C2 iPS-SNS-derived mature oligodendrocytes (MBP⁺). Grafted cells were integrated into myelin sheath. (D) Anti-MBP DAB staining of sagittally sectioned spinal cord of a *shiverer* mouse 8 wk after transplantation. MBP⁺ myelin was detected in the area caudal to the lesion epicenter. (Lower) Higher-magnification image of the boxed area. (E) EM pictures of the injured spinal cord of a 38C2 iPS-SNS-grafted *shiverer* mouse exhibiting a prominent major dense line and intraperiod lines in multiple compacted lamellae. (Scale bars: B, 500 μ m; D Upper, 200 μ m; C and D Lower, 50 μ m; and E, 0.1 μ m.)

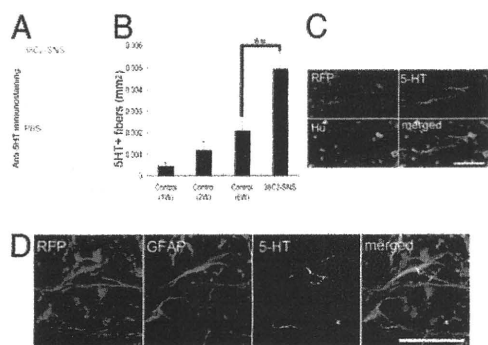


Fig. 4. SNSs derived from a safe MEF-iPS clone promote serotonergic innervation of the dorsal cord and result in better functional recovery of the hindlimbs. (A) 38C2 iPS-SNS transplantation promoted the growth of 5HT⁺ serotonergic fibers in the distal spinal cord. Axial sections of 38C2 iPS-SNS-transplanted (Upper) and PBS control mice (Lower). (B) Quantitative analysis of 5HT⁺ serotonergic fibers of distal cord in the PBS control (1, 2, and 6 wk postinjury) and 38C2 iPS-SNS transplantation groups (6 wk postinjury; 1 and 2 wk postinjury, $n = 3$ each; 6 wk postinjury and 38C2 SNS, $n = 7$ each; $**P < 0.01$). (C and D) Immunohistochemistry of 38C2 iPS-SNS-derived neurons (C, RFP, Hu⁺) and astrocytes (D, RFP, GFAP) closely associated with 5HT⁺ serotonergic fibers. (Scale bars: A, 100 μm ; C, 20 μm ; D, 50 μm .)

of adult tissue-derived iPS cells. Among six TTF-iPS clones pre-evaluated in our previous study (27), we used the safe 335D1 TTF-iPS clone, which was generated with *Nanog* selection and without the transduction of *c-Myc*. We also used the unsafe 256H13 and 256H18 TTF-iPS clones (22, 27), which were generated without genetic selection or the transduction of *c-Myc*, and were originally established from CAG-EGFP mice (22). A subclone of RF8 ES cells carrying the *Nanog*-EGFP reporter (1A2) (19) was used as control. All of the TTF-iPS clones formed PNSs and SNSs (Fig. 5A), and generated cells of all three neural lineages, similar to those derived from 1A2 ES cells (Fig. 5B). We transplanted these TTF-iPS-derived SNSs into injured spinal cords 9 d after injury. Transplantation of the safe 335D1 iPS-SNS (prelabeled with RFP lentivirally) resulted in better functional recovery compared with the PBS control group, without any apparent tumorigenesis during our observation period (Fig. 5C and D). Grafted and survived RFP⁺ 335D1 iPS-SNS-derived cells could differentiate into neural trilineages (Fig. S7A and B). Furthermore, LFB staining revealed that 335D1 iPS-SNS-grafted mice had a significantly larger myelinated area at the lesion epicenter than the PBS control mice at 42 d after injury (Fig. S8A and B), and grafted RFP⁺ 335D1 SNS-derived cells differentiated into MBP⁺ oligodendrocytes (Fig. S8C). However, all unsafe 256H18 iPS-SNS-grafted mice and one of 256H13 iPS-SNS-grafted mice formed teratomas containing EGFP⁺ donor cells within the injured spinal cord (Fig. 5E and F and Fig. S7C). Histological analyses revealed that these teratomas contained epithelial and smooth muscle tissue (Fig. S9A), and also exhibited Nanog immunoreactivity (Fig. 5G). Although the motor functions gradually recovered in both groups to the same extent as in the safe 335D1 iPS-SNS recipients until 35 d after injury, the 256H18 iPS-SNS-grafted animals exhibited a sudden deterioration of motor function 42 d after injury. In contrast, the 256H13 iPS-SNS-grafted animals maintained their functional recovery at 42 d after injury (Fig. 5C). Notably, in most mice of the 256H13 iPS-SNS group, scattered small clusters of Nanog⁺ cells were observed in the spinal cords without obvious teratoma formation (Fig. S9B and C). Thus, we speculate that teratoma formation and subsequent deterioration of function recovery would occur in the 256H13 group if a longer observation period was set.

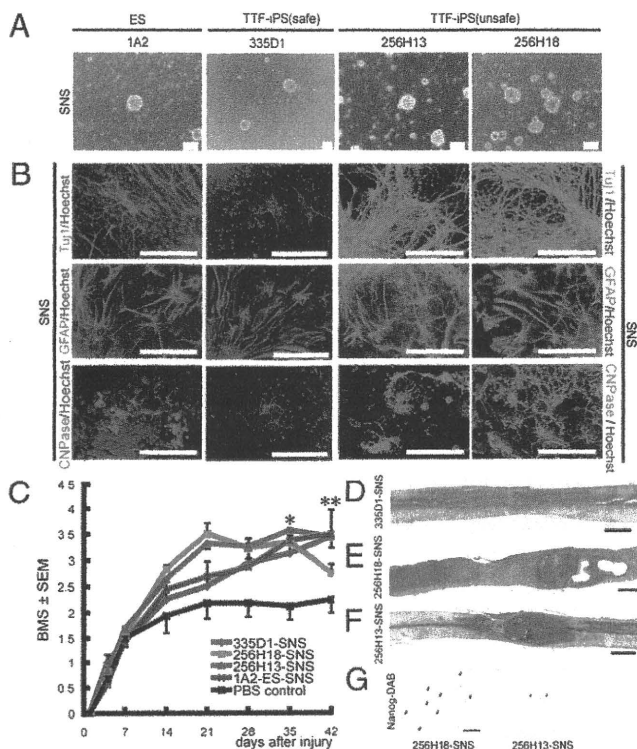


Fig. 5. Characterization and transplantation of SNSs derived from safe and unsafe TTF-iPS cells. (A) Neurospheres derived from 1A2 ES cells, 335D1, 256H13, and 256H18 iPS cells. (Scale bar: 200 μm .) (B) The differentiation potential of TTF-iPS-derived SNSs tested *in vitro* by immunocytochemical analyses of neural cell markers; Tuj1 for neurons, GFAP for astrocytes, and CNPase for oligodendrocytes. (Scale bar: 100 μm .) (C) Time course of functional recovery of the hindlimbs evaluated by BMS. 335D1 iPS-SNS: $n = 9$ each; 256H13 and 256H18 iPS-SNS: $n = 9$; 1A2 ES-SNS: $n = 9$; PBS control: $n = 8$. $*P < 0.05$, $**P < 0.01$. (D–F) H&E sagittal sections of the spinal cord 42 d after injury. (D) 335D1 iPS-SNS, (E) 256H18 iPS-SNS, and (F) 256H13 iPS-SNS grafted mice. There was no evidence of tumorigenesis in the 335D1 iPS-SNS grafted mice (D), whereas teratoma formation was detected within the injured spinal cord in both 256H18 iPS-SNS (E), and 256H13 iPS-SNS (F) grafted mice. (G) Anti-Nanog DAB staining of sagittally sectioned spinal cord of 256H18 and 256H13 iPS-SNS-transplanted animals 35 d after transplantation.

Discussion

In the present study, we showed that the pre-evaluated safe iPS cells could produce neurospheres containing NS/PCs (Fig. 1A) that give rise to trilineage neural cells, including several types of neurons (Fig. 1B and C), and that the neurons were electrophysiologically functional *in vitro* similar to ES cells (Fig. S2).

Based on these safety assessments and *in vitro* findings, we performed an *in vivo* study using the safe 38C2 MEF-iPS cell clone. Grafted 38C2 iPS-SNSs differentiated into neurons, astrocytes, and oligodendrocytes without forming teratomas or other tumors, and promoted functional recovery after SCI, whereas 38C2 iPS-PNSs did not show any therapeutic effects (Fig. 3A). These findings were compatible with our recent data on mouse ES cell-derived neurosphere transplantation into an identical mouse SCI model (31). Transplantation of ES-derived SNSs, which can differentiate into neural trilineages, promoted remyelination, axonal regrowth and tissue sparing, leading to improved function. In contrast, predominantly neurogenic PNSs showed no therapeutic effects on SCI (31). Thus, we elected to use iPS-SNSs and not iPS-PNSs for this study. In fact, the grafted 38C2 iPS-SNSs formed MBP⁺ myelin sheaths within the injured spinal cord. We also confirmed the myelination potential of 38C2 iPS-SNS-derived cells in the spinal cord of the MBP-null *shiverer* mouse by electron microscopy (Fig. 3

D and E). These findings suggested the possibility of the remyelination of demyelinated axons by the grafted 38C2 iPS-SNS-derived oligodendrocytes, which may have contributed to the functional recovery of the grafted animals.

Another potential mechanism for functional recovery is axonal regrowth supported by iPS-SNS-derived astrocytes. Here, we observed grafted 38C2 iPS-SNS-derived GFAP⁺ astrocytes, which exhibited a bipolar morphology with long processes extending along the axis of the spinal cord, caudal to the lesion epicenter, in close association with 5HT⁺ host serotonergic fibers (Fig. 4D). A previous report indicated that immature astrocytes derived from cells grafted into the injured spinal cord promote the outgrowth of 5HT⁺ fibers by offering a growth-permissive surface (38). Consistent with this finding, the transplantation of 38C2 iPS-SNSs promoted serotonergic innervation of the distal cord compared with the PBS control animals, thereby enhancing functional recovery after SCI (Fig. 4A and B) (36). Furthermore, trophic factors, such as neurotrophin-3 (NT-3) and brain-derived neurotrophic factor (BDNF), were expressed in 38C2 iPS-SNSs, which could act as an integral part of the observed functional recovery (39, 40). The tissue sparing (e.g., neuroprotection, axon sprouting and remyelination) and other effects, including functional remodeling of spinal locomotor circuits (41), of trophic factors secreted from grafted cells are considered to be important for functional recovery (42). Thus, the combined effects of the 38C2 iPS-SNS-derived glial cells probably contributed to locomotor function recovery.

For clinical applications, the findings with TTF-iPS cells were promising, as most SCI patients are adults. The transplantation of SNSs derived from a pre-evaluated safe TTF-iPS clone promoted functional recovery after SCI without teratoma formation, like the SNSs from safe MEF-iPS clone did (Fig. 5D). However, the transplantation of SNSs derived from the unsafe TTF-iPS cells resulted in teratoma formation and functional deterioration. The teratoma-forming activity of TTF-iPS-SNSs could be caused by the presence of undifferentiated cells that might be resistant to differentiation signals within the SNSs (27). In fact, we recently reported that persistent presence of undifferentiated cells within iPS-SNSs highly correlated with teratoma-forming propensity, assayed by flow cytometric analysis using *Nanog*-EGFP reporter and transplantation into the brains of immunodeficient (NOD/SCID) (27). Before iPS cells of adult origin can be used clinically, important hurdles must still be overcome. Though new methods for establishing iPS cells are constantly being developed, including virus-free (43) and transgene-free (44) systems, a new strategy is needed to exclude undifferentiated cells from the differentiated progeny of iPS cells. These findings show that the pre-evaluation of iPS cells' *in vitro* differentiation potential could play a critical role in terms of their safety and therapeutic effects on the mouse SCI model. Thus, iPS-derived neurosphere transplantation has potential therapeutic use in SCI, when the iPS cell clones are carefully pre-evaluated.

From a clinical viewpoint, it is particularly encouraging that delaying the iPS-derived NS/PC transplantation (to 9 d after injury) enhanced both the survival of the grafted cells and functional recovery, the therapeutic effects of which is almost comparable to those of fetal CNS-derived NS/PCs transplantation (refs. 34 and 45). This finding may also be applicable to the treatment of patients with SCI. Since our first report of iPS cells (18), there has been increasing interest in their characteristics and therapeutic potential. Our present study demonstrates the therapeutic potential of iPS-derived NS/PCs for SCI repair. Before any clinical trial of human CNS disorders using iPS cells, it will be essential to pre-evaluate each iPS cell clone carefully to guarantee a safety level equal to other types of cells, such as Schwann cells (46, 47) and fetal-derived neurosphere cells (NS/PCs) (3), and to conduct preclinical transplantation studies using appropriate primate models (48, 49).

Methods

Reverse-Transcription and RT-PCR. RNA was isolated with TRIzol (Invitrogen) according to the manufacturer's instructions. Total RNA (0.5 µg) was treated with TURBO DNase (Ambion) and then reverse-transcribed with oligo (dT) primer and SuperScript III (Invitrogen). The primers and PCR conditions used in this study are listed Table S1.

Cell Culture, Neural Induction, and Immunocytochemistry. Mouse ES and iPS cells were cultured as described previously (19, 28, 29). Mouse ES and iPS cells were differentiated into neurospheres via EBs treated with 10⁻⁸ M retinoic acid (Sigma), as described previously with minor modification (28, 29). (Detailed differentiation protocol is described in *SI Text*.) ES and iPS cell-derived neurospheres were dissociated and differentiated on poly-L-ornithine/fibronectin-coated coverslips for 5 d and subjected to immunocytochemical analysis. The number of cells immunoreactive for each marker was counted and shown as the percentage of the total number of cells counterstained with Hoechst 33258. The antibodies used in this study are listed in Table S2.

Lentivirus Production and Infection of Secondary Neurospheres. For BLI tracing of grafted 38C2 iPS-SNSs, we generated a modified lentivirus vector encoding both the click beetle red luciferase (*CBRLuc*; Promega) and mRFP, pCII-EF-CBRLuc-IRES2-mRFP (32, 33). For lentivirus preparation, HEK-293T cells were transfected with pCII-EF-CBRLuc-IRES2-mRFP, pCAG-HIVgp, and pCMV-V5V-G-RSV-Rev, and the conditioned medium containing virus particles was concentrated and used for viral transduction.

Spinal Cord Injury Model and Transplantation. Adult female C57BL/6J mice (20–22 g) were anesthetized via an i.p. injection of ketamine (100 mg/kg) and xylazine (10 mg/kg). A contusive spinal cord injury using an Infinite Horizon Impactor (60 kdyn; Precision Systems) was induced at the Th10 level as reported previously (34). For transplantation, 5 × 10⁵ cells of mouse ES/iPS cell-derived neurospheres, adult dermal fibroblasts in 2 µL of cell suspension, or PBS was injected into the lesion epicenter. Hindlimb motor function was evaluated by the locomotor rating of the Basso mouse scale (BMS) (50) for 42 d after injury. For the *in vivo* imaging of intact and injured spinal cords after the transplantation, a Xenogen-IVIS 100 cooled CCD optical macroscopic imaging system (SC BioScience) was used for BLI, as reported previously (34) (*SI Text*). All procedures were approved by the ethics committee of Keio University, and were in accordance with the Guide for the Care and Use of Laboratory Animals (National Institutes of Health). Grafted animals were deeply anesthetized and intracardially perfused with 4% paraformaldehyde (PFA; pH 7.4). The dissected spinal cords were sectioned into 20-µm axial/sagittal sections using a cryostat and processed for histological analyses. Detailed conditions for histological analyses are described in *SI Text*.

Statistical Analysis. All data are reported as the mean ± SEM. An unpaired two-tailed Student's *t* test was used for the analyses of *in vitro* and *in vivo* 38C2 iPS-SNS and ES-SNS differentiation efficiency (Figs. 1C and 2E), 5HT⁺ areas (Fig. 4B), and LFB⁺ areas (Fig. 2B). Repeated-measures two-way ANOVA, followed by the Tukey–Kramer test, was used for BMS analysis. **P* < 0.05, ***P* < 0.01.

ACKNOWLEDGMENTS. We thank Drs. H. Abe, T. Sunabori, F. Renault-Mihara, W. Akamatsu, S. Shibata, T. Harada, S. Miyao, and H. J. Okano (Keio University) for technical assistance and scientific discussions, and all the members of Dr. Okano's and Dr. Yamanaka's laboratories for encouragement and generous support. We also thank Drs. K. Okita, M. Koyanagi, and K. Tanabe (Kyoto University) for the undifferentiated iPS cells, Dr. H. Niwa (Riken CDB) for the RB3 ES cells, Dr. R. Farese (University of California-San Francisco) for the RB3 ES cells, Dr. R. Y. Tsien (University of California-San Diego) for the mRFP gene, Dr. A. Miyawaki (Riken BSI) for the Venus gene, Dr. H. Baba (Tokyo University of Pharmacy and Life Science) for the shiverer mice, and Dr. H. Miyoshi (Riken BRC) for the lentiviral vectors. We especially thank Drs. S. Okada (Kyushu University), A. Iwanami (University of California-San Francisco and Keio University), and J. Yamane (Keio University) for scientific discussions, technical advice, and encouragement. This work was supported by grants from the Program for Promotion of Fundamental Studies in Health Sciences of the National Institute of Biomedical Innovation (NIBIO), a grant from Uehara Memorial Foundation, and Grants-in-Aid for Scientific Research from the Japan Society for the Promotion of Science (JSPS) and the Ministry of Education, Culture, Sports, Science and Technology of Japan (MEXT), the project for realization of regenerative medicine and support for the core institutes for iPS cell research from MEXT; Japan Science and Technology Agency (SORST); the Ministry of Health, Labor, and Welfare; the General Insurance Association of Japan; Research Fellowships for Young Scientists from the Japan Society for the Promotion of Science; Keio Gijuku Academic Development Funds; and a Grant-in-aid for the Global COE program from MEXT to Keio University.

1. Björklund A, Lindvall O (2000) Cell replacement therapies for central nervous system disorders. *Nat Neurosci* 3:537–544.
2. Okano H (2002) Stem cell biology of the central nervous system. *J Neurosci Res* 69: 698–707.
3. Lindvall O, Kokaia Z, Martinez-Serrano A (2004) Stem cell therapy for human neurodegenerative disorders—how to make it work. *Nat Med* 10 (Suppl):S42–S50.
4. Martino G, Pluchino S (2006) The therapeutic potential of neural stem cells. *Nat Rev Neurosci* 7:395–406.
5. Lindvall O, Kokaia Z (2006) Stem cells for the treatment of neurological disorders. *Nature* 441:1094–1096.
6. Gage FH (2000) Mammalian neural stem cells. *Science* 287:1433–1438.
7. Wichterle H, Lieberam I, Porter JA, Jessell TM (2002) Directed differentiation of embryonic stem cells into motor neurons. *Cell* 110:385–397.
8. Watanabe K, et al. (2005) Directed differentiation of telencephalic precursors from embryonic stem cells. *Nat Neurosci* 8:288–296.
9. Sonntag KC, et al. (2007) Enhanced yield of neuroepithelial precursors and midbrain-like dopaminergic neurons from human embryonic stem cells using the bone morphogenic protein antagonist noggin. *Stem Cells* 25:411–418.
10. Tropepe V, et al. (2001) Direct neural fate specification from embryonic stem cells: A primitive mammalian neural stem cell stage acquired through a default mechanism. *Neuron* 30:65–78.
11. Ying QL, Stavridis M, Griffiths D, Li M, Smith A (2003) Conversion of embryonic stem cells into neuroectodermal precursors in adherent monoculture. *Nat Biotechnol* 21: 183–186.
12. McDonald JW, et al. (1999) Transplanted embryonic stem cells survive, differentiate and promote recovery in injured rat spinal cord. *Nat Med* 5:1410–1412.
13. Brüstle O, et al. (1999) Embryonic stem cell-derived glial precursors: A source of myelinating transplants. *Science* 285:754–756.
14. Kim JH, et al. (2002) Dopamine neurons derived from embryonic stem cells function in an animal model of Parkinson's disease. *Nature* 418:50–56.
15. Sharp J, Keirstead HS (2007) Therapeutic applications of oligodendrocyte precursors derived from human embryonic stem cells. *Curr Opin Biotechnol* 18:434–440.
16. Keirstead HS, et al. (2005) Human embryonic stem cell-derived oligodendrocyte progenitor cell transplants remyelinate and restore locomotion after spinal cord injury. *J Neurosci* 25:4694–4705.
17. Hochedlinger K, Jaenisch R (2006) Nuclear reprogramming and pluripotency. *Nature* 441:1061–1067.
18. Takahashi K, Yamanaka S (2006) Induction of pluripotent stem cells from mouse embryonic and adult fibroblast cultures by defined factors. *Cell* 126:663–676.
19. Okita K, Ichisaka T, Yamanaka S (2007) Generation of germline-competent induced pluripotent stem cells. *Nature* 448:313–317.
20. Wernig M, et al. (2007) In vitro reprogramming of fibroblasts into a pluripotent ES-cell-like state. *Nature* 448:318–324.
21. Maherali N, et al. (2007) Directly reprogrammed fibroblasts show global epigenetic remodeling and widespread tissue contribution. *Cell Stem Cell* 1:55–70.
22. Nakagawa M, et al. (2008) Generation of induced pluripotent stem cells without Myc from mouse and human fibroblasts. *Nat Biotechnol* 26:101–106.
23. Wernig M, Meissner A, Cassidy JP, Jaenisch R (2008) c-Myc is dispensable for direct reprogramming of mouse fibroblasts. *Cell Stem Cell* 2:10–12.
24. Hanna J, et al. (2007) Treatment of sickle cell anemia mouse model with iPS cells generated from autologous skin. *Science* 318:1920–1923.
25. Wernig M, et al. (2008) Neurons derived from reprogrammed fibroblasts functionally integrate into the fetal brain and improve symptoms of rats with Parkinson's disease. *Proc Natl Acad Sci USA* 105:5856–5861.
26. Yamanaka S (2007) Strategies and new developments in the generation of patient-specific pluripotent stem cells. *Cell Stem Cell* 1:39–49.
27. Miura K, et al. (2009) Variation in the safety of induced pluripotent stem cell lines. *Nat Biotechnol* 27:743–745.
28. Okada Y, et al. (2008) Spatiotemporal recapitulation of central nervous system development by murine embryonic stem cell-derived neural stem/progenitor cells. *Stem Cells* 26:3086–3098.
29. Okada Y, Shimazaki T, Sobue G, Okano H (2004) Retinoic-acid-concentration-dependent acquisition of neural cell identity during in vitro differentiation of mouse embryonic stem cells. *Dev Biol* 275:124–142.
30. Niwa H, Miyazaki J, Smith AG (2000) Quantitative expression of Oct-3/4 defines differentiation, dedifferentiation or self-renewal of ES cells. *Nat Genet* 24:372–376.
31. Kumagai G, et al. (2009) Roles of ES cell-derived gliogenic neural stem/progenitor cells in functional recovery after spinal cord injury. *PLoS ONE* 4:e7706.
32. Masuda H, et al. (2007) Noninvasive and real-time assessment of reconstructed functional human endometrium in NOD/SCID/gamma c(null) immunodeficient mice. *Proc Natl Acad Sci USA* 104:1925–1930.
33. Miyoshi H, Blömer U, Takahashi M, Gage FH, Verma IM (1998) Development of a self-inactivating lentivirus vector. *J Virol* 72:8150–8157.
34. Okada S, et al. (2005) In vivo imaging of engrafted neural stem cells: Its application in evaluating the optimal timing of transplantation for spinal cord injury. *FASEB J* 19: 1839–1841.
35. Inoue Y, et al. (1986) Alteration of the primary pattern of central myelin in a chimaeric environment—study of shiverer ↔ wild-type chimaeras. *Brain Res* 391:239–247.
36. Bregman BS, et al. (1993) Recovery of function after spinal cord injury: Mechanisms underlying transplant-mediated recovery of function differ after spinal cord injury in newborn and adult rats. *Exp Neurol* 123:3–16.
37. Nygren LG, Fuxe K, Jonsson G, Olson L (1974) Functional regeneration of 5-hydroxytryptamine nerve terminals in the rat spinal cord following 5, 6-dihydroxytryptamine induced degeneration. *Brain Res* 78:377–394.
38. Hofstetter CP, et al. (2002) Marrow stromal cells form guiding strands in the injured spinal cord and promote recovery. *Proc Natl Acad Sci USA* 99:2199–2204.
39. Widenfalk J, Lundströmer K, Jubran M, Brene S, Olson L (2001) Neurotrophic factors and receptors in the immature and adult spinal cord after mechanical injury or kainic acid. *J Neurosci* 21:3457–3475.
40. McTigue DM, Horner PJ, Stokes BT, Gage FH (1998) Neurotrophin-3 and brain-derived neurotrophic factor induce oligodendrocyte proliferation and myelination of regenerating axons in the contused adult rat spinal cord. *J Neurosci* 18:5354–5365.
41. Courtine G, et al. (2009) Transformation of nonfunctional spinal circuits into functional states after the loss of brain input. *Nat Neurosci* 12:1333–1342.
42. Lu P, Tuszynski MH (2008) Growth factors and combinatorial therapies for CNS regeneration. *Exp Neurol* 209:313–320.
43. Okita K, Nakagawa M, Hyenjong H, Ichisaka T, Yamanaka S (2008) Generation of mouse induced pluripotent stem cells without viral vectors. *Science* 322:949–953.
44. Zhou H, et al. (2009) Generation of induced pluripotent stem cells using recombinant proteins. *Cell Stem Cell* 4:381–384.
45. Ogawa Y, et al. (2002) Transplantation of in vitro-expanded fetal neural progenitor cells results in neurogenesis and functional recovery after spinal cord contusion injury in adult rats. *J Neurosci Res* 69:925–933.
46. Pearce DD, et al. (2004) cAMP and Schwann cells promote axonal growth and functional recovery after spinal cord injury. *Nat Med* 10:610–616.
47. Pearce DD, et al. (2007) Transplantation of Schwann cells and/or olfactory ensheathing glia into the contused spinal cord: Survival, migration, axon association, and functional recovery. *Glia* 55:976–1000.
48. Iwanami A, et al. (2005) Establishment of graded spinal cord injury model in a nonhuman primate: The common marmoset. *J Neurosci Res* 80:172–181.
49. Iwanami A, et al. (2005) Transplantation of human neural stem cells for spinal cord injury in primates. *J Neurosci Res* 80:182–190.
50. Basso DM, et al. (2006) Basso Mouse Scale for locomotion detects differences in recovery after spinal cord injury in five common mouse strains. *J Neurotrauma* 23:635–659.

Antiapoptotic and Antiautophagic Effects of Glial Cell Line-Derived Neurotrophic Factor and Hepatocyte Growth Factor After Transient Middle Cerebral Artery Occlusion in Rats

Jingwei Shang,¹ Kentaro Deguchi,¹ Toru Yamashita,¹ Yasuyuki Ohta,¹
Hanzhe Zhang,¹ Nobutoshi Morimoto,¹ Ning Liu,¹ Xuemei Zhang,¹
Fengfeng Tian,¹ Tohru Matsuura,¹ Hiroshi Funakoshi,²
Toshikazu Nakamura,³ and Koji Abe^{1*}

¹Department of Neurology, Okayama University Graduate School of Medicine, Dentistry and Pharmaceutical Sciences, Okayama, Japan

²Division of Molecular Regenerative Medicine, Department of Biochemistry and Molecular Biology, Osaka University Graduate School of Medicine, Osaka, Japan

³Kringle Pharma Joint Research Division for Regenerative Drug Discovery, Center for Advanced Medicine, Osaka University, Osaka, Japan

Glial cell line-derived neurotrophic factor (GDNF) and hepatocyte growth factor (HGF) are strong neurotrophic factors, which function as antiapoptotic factors. However, the neuroprotective effect of GDNF and HGF in ameliorating ischemic brain injury via an antiautophagic effect has not been examined. Therefore, we investigated GDNF and HGF for changes of infarct size and antiapoptotic and antiautophagic effects after transient middle cerebral artery occlusion (tMCAO) in rats. For the estimation of ischemic brain injury, the infarct size was calculated at 24 hr after tMCAO by HE staining. Terminal deoxynucleotidyl transferase-mediated dUTP-biotin in situ nick end labeling (TUNEL) was performed for evaluating the antiapoptotic effect. Western blot analysis of microtubule-associated protein 1 light chain 3 (LC3) and immunofluorescence analysis of LC3 and phosphorylated mTOR/Ser²⁴⁴⁸ (p-mTOR) were performed for evaluating the antiautophagic effect. GDNF and HGF significantly reduced infarct size after cerebral ischemia. The amounts of LC3-I plus LC3-II (relative to β -tubulin) were significantly increased after tMCAO, and GDNF and HGF significantly decreased them. GDNF and HGF significantly increased p-mTOR-positive cells. GDNF and HGF significantly decreased the numbers of TUNEL-, LC3-, and LC3/TUNEL double-positive cells. LC3/TUNEL double-positive cells accounted for about 34.3% of LC3 plus TUNEL-positive cells. This study suggests that the protective effects of GDNF and HGF were greatly associated with not only the antiapoptotic but also the antiautophagic effects; maybe two types of cell death can occur in the same cell at the same time, and GDNF and HGF are capable of ameliorating these two pathways. © 2010 Wiley-Liss, Inc.

Key words: apoptosis; autophagy; GDNF; HGF; cerebral ischemia

In ischemic diseases, ischemic severity and duration lead to cell death and determine tissue pathology (Cotran et al., 1998). In recent years, new types of cell death have been described; three types of cell deaths have been distinguished mainly by morphological criteria. Type I cell death is better known as apoptosis, and autophagic vacuoles inside the dying cell are typical for type II cell death, whereas type III cell death (better known as necrosis) is distinguished by early plasma membrane rupture and dilation of cytoplasmic organelles (Kroemer, 2005; Galluzzi, 2007; Feig and Peter, 2007). Apoptosis is associated with nuclear and chromatin condensation, DNA fragmentation, organelle swelling, cytoplasmic vacuolization, and nuclear envelope disruption (Kerr et al., 1972; Green and Kroemer, 1998). Autophagy is a regulated process of degradation and recycling of cellular

Contract grant sponsor: Ministry of Education, Science, Culture and Sports of Japan; Contract grant number: 21390267; Contract grant sponsor: Research Committee of CNS Degenerative Diseases (to I. Nakano); Contract grant sponsor: Ministry of Health, Labour and Welfare of Japan (to Y. Itoyama, T. Imai).

*Correspondence to: Koji Abe, Okayama University Graduate School of Medicine, Dentistry and Pharmaceutical Sciences, 2-5-1 Shikatacho, Okayama 700-8558, Japan. E-mail: abekabek@cc.okayama-u.ac.jp

Received 7 November 2009; Revised 5 December 2009; Accepted 26 December 2009

Published online 19 February 2010 in Wiley InterScience (www.interscience.wiley.com). DOI: 10.1002/jnr.22373

constituents, participating in organelle turnover and in the bioenergetic management of starvation (Kabeya et al., 2000; Klionsky and Emr, 2000; Inbal et al., 2002; Reggiori and Klionsky, 2002; Klionsky et al., 2003; Yoshimori, 2004). Recently, 27 autophagy-related (ATG) genes were identified whose products appear to be related to the autophagy process. These genes were characterized in yeast (Klionsky et al., 2003; Yorimitsu and Klionsky, 2005). For example, rat microtubule-associated protein 1 light chain 3 (LC3), a mammalian homologue of Atg8, plays a critical role in the formation of autophagosomes (Kirisako et al., 1999).

Glial cell line-derived neurotrophic factor (GDNF), a member of the transforming growth factor- β superfamily (Lin et al., 1993), has a potent neuroprotective effect on a variety of neuronal damage both in vitro and in vivo (Lin et al., 1993, 1995; Beck et al., 1995; Tomac et al., 1995; Henderson et al., 1997). We and others have reported that topical application and intracerebral administration of GDNF decreased the size of ischemia-induced brain infarction and the number of TUNEL-positive neurons with suppressing apoptotic pathways such as caspases-1 and -3 (Abe et al., 1997; Wang et al., 1997; Kitagawa et al., 1998).

Hepatocyte growth factor (HGF) is a multifunctional growth factor originally identified as a potent mitogen for hepatocytes in primary culture (Nakamura et al., 1984; Russell et al., 1984). HGF specifically binds and activates a tyrosine kinase receptor encoded by the *c-Met* protooncogene (Bottaro et al., 1991). Both HGF and *c-Met* were reported to be expressed in both adult and fetal central nervous system (Matsumoto and Nakamura, 1997; Maina and Klein, 1999). HGF plays important roles in mitogenesis, motogenesis, morphogenesis, antiapoptosis, and angiogenesis (Nakamura et al., 1989; Zarnegar and Michalopoulos, 1995; Matsumoto and Nakamura, 1996; Maina et al., 1998; Van Belle et al., 1998). In the brain, HGF has the functions of a neurotrophic factor via promotion of antiapoptosis, neurite extension, and migration; a modulatory factor for glial cell numbers and function; and an angiogenic factor (Honda et al., 1995; Van Belle et al., 1998; Miyazawa et al., 1998; Sun et al., 2002). We and others have reported that intraventricular and intracerebral administration of HGF protein or transplantation of bone marrow stromal cells with ex vivo HGF gene transfer decreased the size of ischemia-induced brain infarction (Miyazawa et al., 1998; Zhao et al., 2006) and the number of TUNEL-positive neurons with increasing presentation of Bcl-2 (Tsuzuki et al., 2001). In addition, HGF also plays a role in attenuating ischemia-induced brain infarction via caspase-independent cascade by preventing apoptosis-inducing factor (AIF) translocation downstream of poly(ADP-ribose) polymerase (PARP) and p53 (Niimura et al., 2006a,b).

However, the antiautophagic effect of GDNF and HGF in ameliorating ischemic brain injury has not yet been documented. In this study, we examined the antiapoptotic and antiautophagic effects of GDNF and HGF after tMCAO in rats.

MATERIALS AND METHODS

Surgical Preparation

Adult male Wistar rats (SLC, Shizuoka, Japan) weighing 250–280 g were used for the experiments. The animals were anesthetized with an intraperitoneal injection of 40 mg/kg pentobarbital and positioned in a stereotaxic operating apparatus. A 2-mm-diameter burr hole was carefully made at 3 mm dorsal and 4 mm lateral to the right from bregma using an electric dental drill, avoiding traumatic brain injury. Dura mater was preserved at that time. The location of the burr hole was in the upper part of the right middle cerebral artery (MCA) territory. Then, the incision was closed, and the animals were allowed to free access to water and food at room temperature.

On the next day, at about 24 hr after the drilling, the rats were lightly anesthetized by inhalation of a 69%/30% (v/v) mixture of nitrous oxide/oxygen and 1% halothane using a face mask. A midline neck incision was made and the right common carotid artery exposed, and then inhalation of anesthetics was stopped. When the animal began to regain consciousness, the right MCA was occluded by insertion of 4-0 surgical nylon thread with silicone coating through the common carotid artery (Nagasawa and Kogure, 1989; Abe et al., 1992). With this technique, the tip of the thread occludes the origin of the right MCA. The reliability of producing successful strokes is almost complete in this model (Koizumi et al., 1986). During these procedures, body temperature was monitored with a rectal probe and maintained at $37^{\circ} \pm 0.3^{\circ}\text{C}$ using a heating pad. The surgical incision was then closed, and the animals were allowed to recover at room temperature. After 90 min of MCA occlusion (MCAO), cerebral blood flow (CBF) was restored by removal of the nylon thread.

HGF or GDNF Treatment In Vivo

Just after restoration of CBF, the dura mater under the burr hole was carefully removed, and a small piece (8 mm³) of spongel (Yamanouchi Pharma Co., Ltd.) presoaked in 9 μl Ringer solution (Otsuka Pharma. Co., Ltd.) as vehicle or a solution containing GDNF (3.0 μg in 9 μl of vehicle; Sigma, St. Louis, MO) or HGF (30.0 μg in 9 μl of vehicle; Kringle Pharma) was placed in contact with the surface of the cerebral cortex. In terms of the dose of HGF, 5.0, 10.0, and 30.0 μg were checked in our preliminary experiment (Miyazawa et al., 1998; Niimura et al., 2006a,b), and the effect of 30.0 μg in 9 μl of vehicle was the best among them. The dose of GDNF was chosen based on our previous report (Abe et al., 1997). The spongel was buried in the skull bone. The surface of the skull bone was then covered with vinyl tape, and the head skin incision was closed. It is reported that application of growth factor in spongel is as effective as chronic infusion (Otto et al., 1989). The above-described operations were performed in a sterile fashion. Sham-operated control animals underwent burr hole surgery, exposure of the common carotid artery without MCAO, and placement of spongel presoaked in vehicle. The experimental protocol and procedures were approved by the Animal Committee of Okayama University School of Medicine.

Preparation and Quantitative Analysis of Infarct Volume

The animals ($n = 5$) were sacrificed at 24 hr after the restoration of CBF under deep anesthesia with pentobarbital (10 mg/250 g rat). The rats were transcardially perfused with heparinized saline, followed by 4% paraformaldehyde in phosphate buffer (PB). The whole brain was subsequently removed and immersed in the same fixation for 12 hr at 4°C. After washing out of paraformaldehyde by PB, the brain was immersed in sucrose solution in PB and then rapidly frozen in powdered dry ice and stored at -80°C. Coronal brain sections of 20 μm thickness were prepared by using a cryostat and mounted on a silane-coated glass.

For quantitative analysis of infarct volume, the sections were stained with hematoxylin and eosin (HE) and observed with a light microscope (Olympus BX-51; Olympus Optical). The area of the infarct was measured in five sections by pixel counting using a computer program for Photoshop 7.0, and the volume was calculated.

Western Blot Analysis

Western blot analysis was performed using the infarct hemisphere of five mice from each group. We added 3 ml cold lysis buffer (50 mM Tris-HCl, pH 7.2, 10% glycerol, 250 mM NaCl, 0.1% NP-40, 2 mM EDTA, and protease inhibitors) to the brain tissue and homogenized it at 4°C. The homogenate was centrifuged at 12,000 rpm at 4°C, and the supernatant was used for Western blotting. We carried out Western blot analysis using standard techniques with an ECL Plus detection kit (GE Healthcare). The dilution of the anti-LC3 (Medical Biological Laboratories; No. PD012) antibody was 1:500. We carried out densitometry analysis in Scion Image Beta 4.02 software and took the average of the five mice.

TUNEL Staining

In accordance with our previous report (Abe et al., 1997), TUNEL study was performed using a kit (Roche, Nonnenwald, Germany) that detects double-strand breaks in genomic DNA with diaminobenzidine.

Single Immunofluorescence Analysis

The fresh-frozen sections were fixed for 10 min in ice-cold acetone and air dried. Then, the sections were rinsed three times in PBS (pH 7.4). After blocking with 10% normal rabbit serum for 2 hr, the slides were incubated for 16 hr at 4°C with the first antibody: anti-LC3 antibody (MBL; No. PM046) at 1:200 or anti-p-mTOR antibody (Cell Signaling Technologies, Danvers, MA; No. 2971) at 1:100 diluted in PBS containing 10% normal rabbit serum and 0.3% Triton X-100. To confirm the specificity of the primary antibody, a set of sections was stained in a similar way, without primary antibodies. The sections were then washed and incubated for 2 hr with the second antibody: Texas red-labeled anti-rabbit IgG antibody at 1:200 (Vector, Burlingame, CA) or FITC-labeled anti-rabbit IgG antibody at 1:200 (Vector). The slides were then covered with Vectashield Mounting Medium with 4',6'-diamidino-2-phenylindole (Vector).

Double-Immunofluorescence Analysis

Double-immunofluorescence studies were performed for LC3 plus neuronal nuclear antigen (NeuN) or glial fibrillary acidic protein (GFAP) or TUNEL or N-acetylglucosamine oligomers (NAGO). Lycopersicon esculentum lectin (LEL) is a glycoprotein with affinity for NAGO, which mature vascular endothelial cells express (Augustin et al., 1995). The staining steps were the same as those described above; LEL and the first antibody were chosen with each dilution as follows: anti-LC3 antibody at 1:200, anti-NeuN antibody (Chemicon, Temecula, CA) at 1:200, anti-GFAP antibody (Dako, Carpinteria, CA) at 1:1,000, biotinylated LEL (Vector) at 1:200 diluted in PBS containing 10% normal rabbit serum and 0.3% Triton X-100. The second antibody were Texas red-labeled anti-rabbit IgG antibody at 1:200 (Vector) plus TUNEL enzyme and label or FITC avidin D (Vector) or FITC-labeled secondary antibodies (Vector). The treated sections were scanned with a confocal microscope equipped with an argon and HeNe1 laser (LSM-510; Zeiss, Jena, Germany). Sets of fluorescent images were acquired sequentially for the red and green channels to prevent crossover of signals from green to red or from red to green channels.

Quantitative Analysis

To evaluate the results of TUNEL staining and single-immunofluorescence analysis quantitatively, the positively stained cells were counted in the cerebral cortex at the boundary zone in five coronal sections per rat brain. In the double-fluorescence studies, the double-positive cells and vessels were counted in the same manner. Results are expressed as means \pm SD.

Statistical Analysis

All data are expressed as means \pm SD. One-way ANOVA with post hoc test was used for each evaluation.

RESULTS

Quantitative Analysis of Infarct Volume

Ninety minutes of MCAO caused large infarcts of the lateral cortex and the underlying caudoputamen. Infarct areas of five coronal sections (2, 4, 6, 8, and 10 mm caudal from frontal pole) are shown (Fig. 1a). The infarct volume of the vehicle-treated group was $478.0 \pm 34.8 \text{ mm}^3$ (mean \pm SD), HGF-treated group was $420.0 \pm 23.8 \text{ mm}^3$, and GDNF-treated group was $306.0 \pm 52.2 \text{ mm}^3$. The infarct volume of GDNF (** $P < 0.01$) and HGF (* $P < 0.05$)-treated groups was significantly smaller than that of vehicle-treated group (Fig. 1b).

Antiapoptotic Effect

The TUNEL-positive stained cells were distributed in the cerebral cortex and dorsal caudate of the MCA territory but were not found in other areas of the ipsilateral hemisphere or the contralateral side. The staining was found exclusively in the nuclei of neuronal cells. A strong staining for TUNEL was present in the vehicle-treated group, but the treatment with GDNF (** $P <$

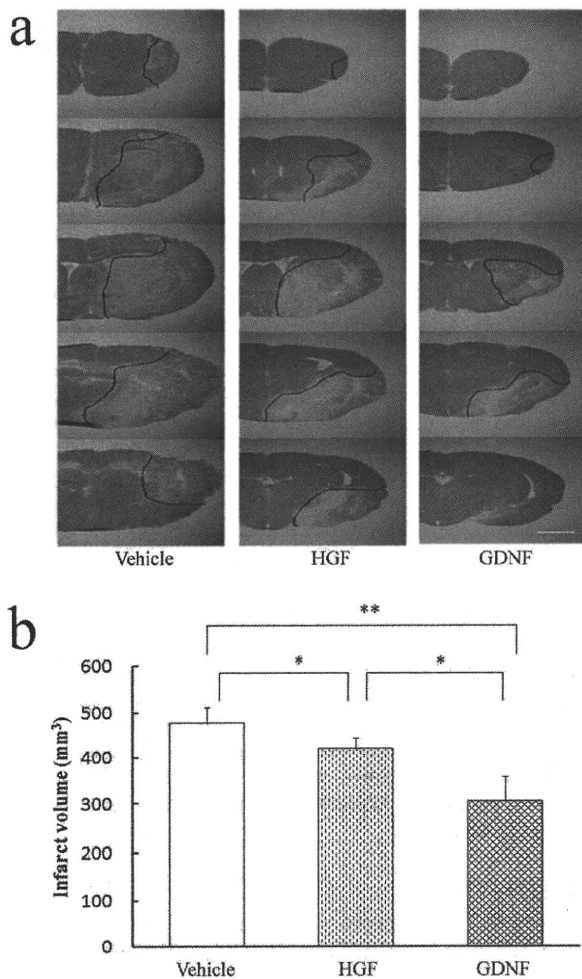


Fig. 1. HE staining (a) and quantitative analysis of infarct volume at 24 hr after the reperfusion (b). The infarct volume of GDNF (** $P < 0.01$)- and HGF (* $P < 0.05$)-treated groups was significantly smaller than that of vehicle-treated group. Scale bar = 5 mm.

0.01) and HGF (* $P < 0.05$) greatly reduced the number of TUNEL-positive cells at 24 hr after 90 min of MCAO: $389.8 \pm 63.7/\text{mm}^2$ in vehicle-treated group, $247.5 \pm 54.5/\text{mm}^2$ in HGF-treated group, $76.2 \pm 32.1/\text{mm}^2$ in GDNF-treated group (mean \pm SD; Fig. 2a,b).

Antiautophagic Effect

Examining the intracellular localization of LC3 in the ischemic brain. Cerebral ischemia induces autophagy (Adhami et al., 2006; Rami et al., 2008). To show whether the protective effects of GDNF and HGF are associated with the antiautophagic effect after cerebral ischemia, we examined the protein level of LC3 in ischemic and normal brains (Fig. 3a). The number of cells displaying punctate LC3 fluorescence significantly

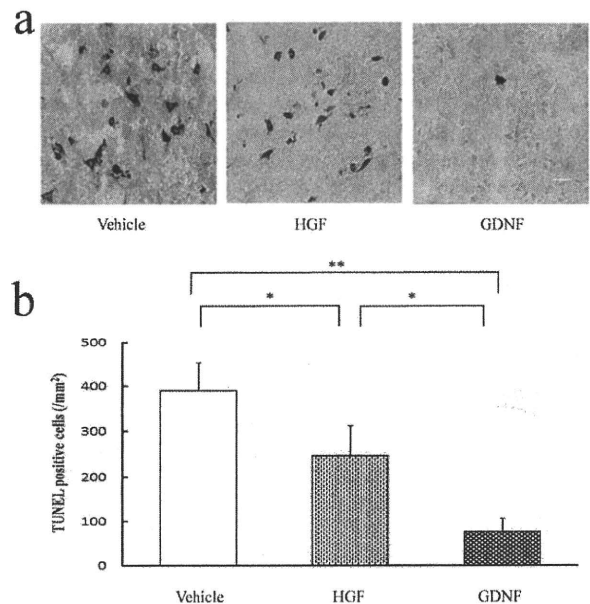


Fig. 2. TUNEL staining (a) and quantitative analysis of TUNEL-positive cells for evaluating antiapoptotic effect at 24 hr after reperfusion (b). A strong staining for TUNEL was present in the vehicle group, but the treatment with GDNF (** $P < 0.01$) and HGF (* $P < 0.05$) greatly reduced the number of TUNEL-positive cells (* $P < 0.05$). Scale bar = 20 μm .

increased after cerebral ischemia, and the numbers in GDNF- and HGF-treated groups significantly decreased compared with the vehicle-treated group ($P < 0.05$; Fig. 3b): $33.5 \pm 5.7/\text{mm}^2$ in sham group, $152.6 \pm 23.4/\text{mm}^2$ in vehicle-treated group, $106.1 \pm 15.9/\text{mm}^2$ in HGF-treated group, $64.7 \pm 19.9/\text{mm}^2$ in GDNF-treated group (mean \pm SD). Double-immunofluorescence studies were performed for LC3 and for various brain cell type markers (NeuN to identify neuronal cells, GFAP to identify astrocytes, and NAGO to identify vascular endothelium cells) after cerebral ischemia. Confocal microscopy analysis of the double-stained sections indicated that LC3 and NeuN or GFAP or NAGO were expressed in the same cell (Fig. 3c). Semiquantitative assessment showed that approximately 57% of LC3-positive cells presented both LC3 and NeuN, 30% presented both LC3 and GFAP, and 13% presented both LC3 and NAGO (Fig. 3d).

Western blot analysis for LC3-I and LC3-II in the infarct hemisphere. The amounts of LC3-I plus LC3-II (relative to β -tubulin) were significantly higher in the vehicle-, HGF-, and GDNF-treated groups than in the sham group ($P < 0.05$), and those in the GDNF- and HGF-treated group significantly decreased compared with the vehicle-treated group ($P < 0.05$): 1.39 ± 0.04 in sham group, 3.15 ± 0.30 in vehicle-treated group, 2.64 ± 0.18 in HGF-treated group, 2.13 ± 0.14 in GDNF-treated group (mean \pm SD). The amounts of

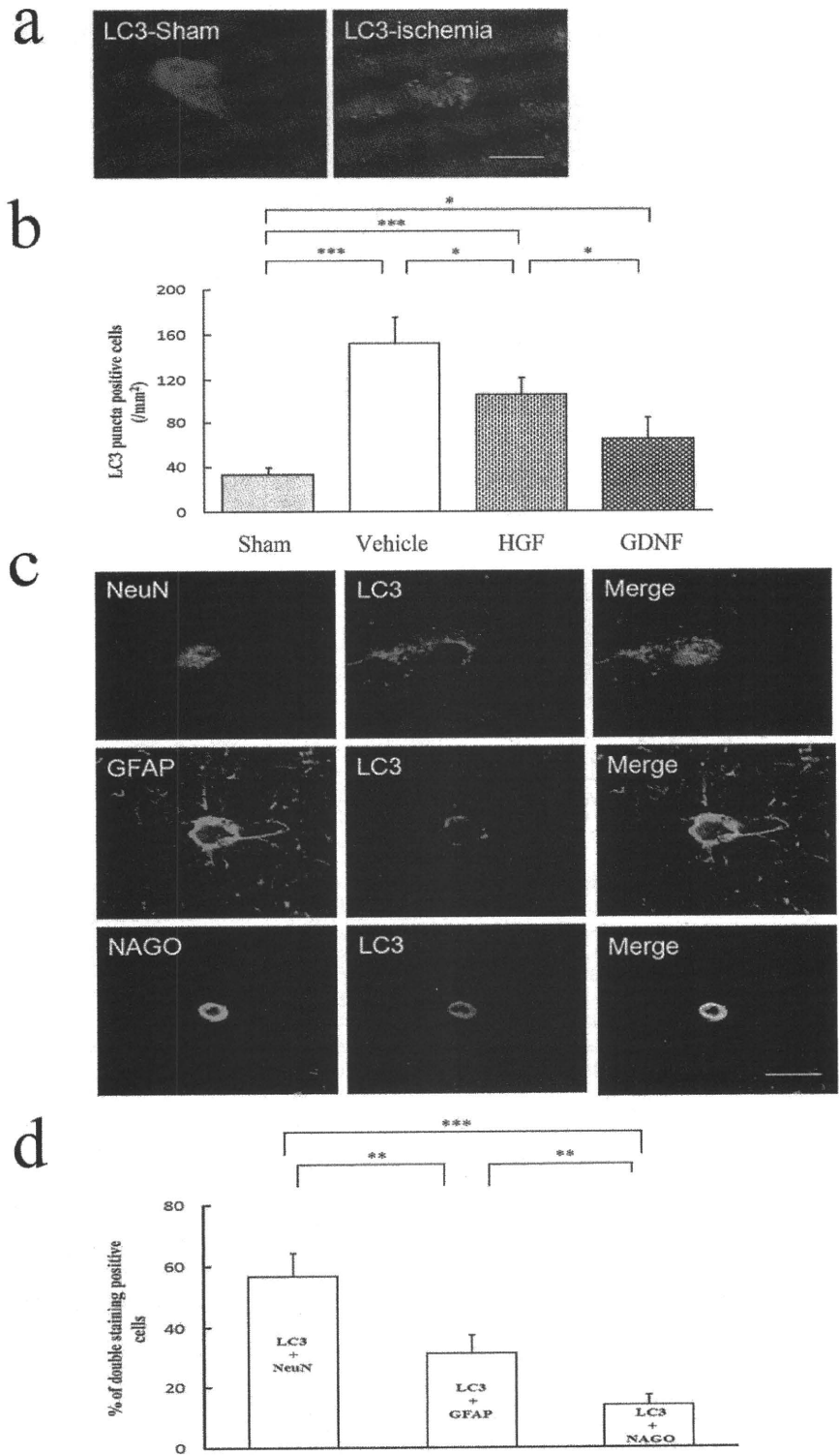


Fig. 3. Immunofluorescence of LC3 in sham and in ischemic brain (a) and quantitative analysis of cells with punctate LC3 fluorescence (b). Double staining of LC3 and NeuN or GFAP or NAGO in ischemic brain (c) and semi-quantitative analysis of cells with LC3 and NeuN or GFAP or NAGO fluorescence (d). The numbers of cells displaying punctate LC3 fluorescence significantly increased after cerebral ischemia ($***P < 0.001$), and the numbers in the GDNF- and HGF-treated groups significantly decreased compared with the vehicle-treated group ($*P < 0.05$). Although LC3 and NeuN or GFAP or NAGO are expressed in the same cell, LC3 is expressed mainly in neurons in the cerebral cortex and dorsal caudate of the MCA territory. Scale bars = 20 μm in a; 20 μm in c.

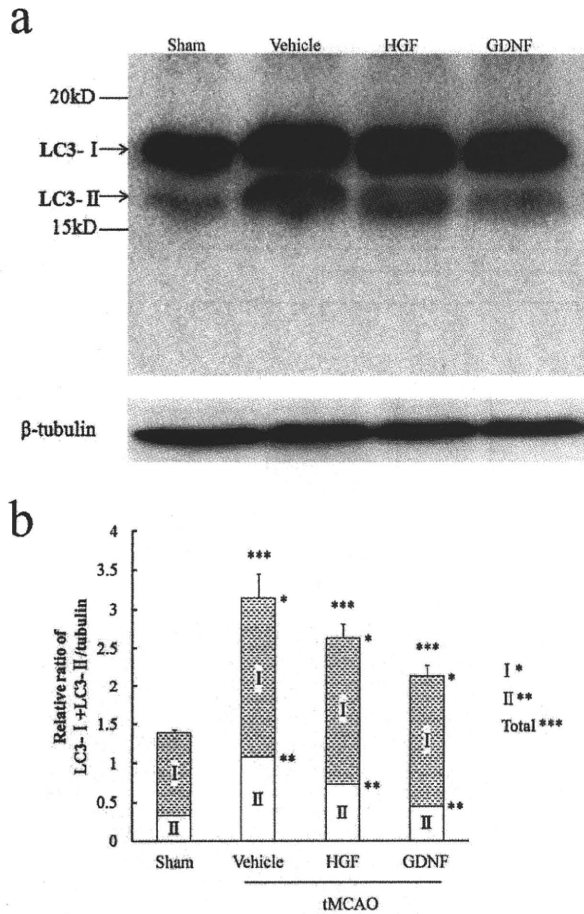


Fig. 4. Western blot analysis of infarct hemisphere for LC3 protein (a) and quantitative analysis relative to β-tubulin (b). The amounts of LC3-I plus LC3-II and LC3-II (relative to β-tubulin) were significantly higher in the vehicle-, HGF-, and GDNF-treated groups than in the sham group ($P < 0.05$), and those of the GDNF- and HGF-treated group significantly decreased compared with the vehicle-treated group ($P < 0.05$). The amounts of LC3-I (relative to β-tubulin) were significantly higher in the vehicle-, HGF-, and GDNF-treated groups than in the sham group ($P < 0.05$), but there was no difference among them. * $P < 0.05$ for LC3-I vs. sham, ** $P < 0.05$ for LC3-II vs. sham, *** $P < 0.01$ for LC3-I plus LC3-II vs. sham.

LC3-I were significantly higher in the vehicle-, HGF-, and GDNF-treated groups than in the sham group ($P < 0.05$), but there was no difference among them. The result for LC3-II change was the same as for LC3-I plus LC3-II (Fig. 4a,b).

Single-immunofluorescence analysis of p-mTOR. Immunofluorescence staining of sections with an antibody against p-mTOR showed that the number of immunopositive neurons in the cerebral cortex and dorsal caudate of the MCA territory significantly increased in the HGF (* $P < 0.05$)- and GDNF (** $P < 0.01$)-treated groups: $414.2 \pm 78.5/\text{mm}^2$ in vehicle-

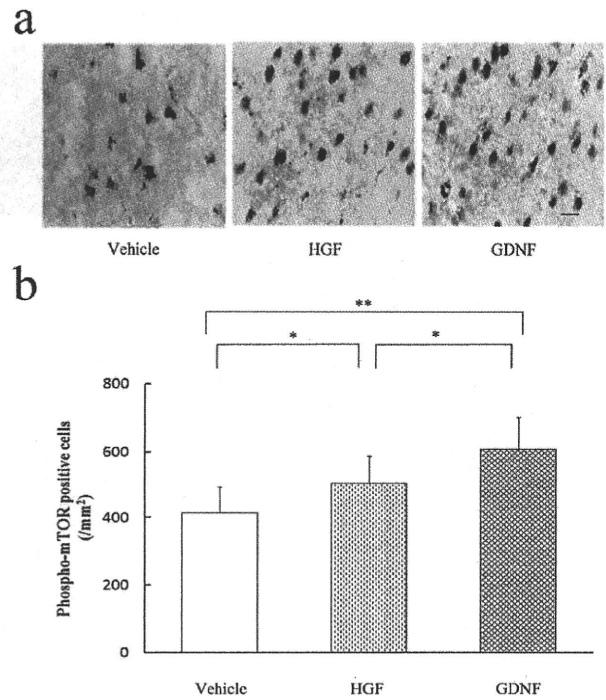


Fig. 5. Immunofluorescence of p-mTOR in the cerebral cortex and dorsal caudate of the MCA territory (a) and quantitative analysis of p-mTOR-positive cells (b). The number of p-mTOR-positive cells significantly increased in the HGF (* $P < 0.05$)- and GDNF (** $P < 0.01$)-treated groups. Scale bar = 20 μm.

treated group, $502.4 \pm 85.2/\text{mm}^2$ in HGF-treated group, $607.4 \pm 96.7/\text{mm}^2$ in GDNF-treated group (mean \pm SD; Fig. 5a,b).

Double-immunofluorescence analysis of LC3/TUNEL staining. Immunofluorescence analysis showed that both LC3 and TUNEL are expressed mainly in neurons in the cerebral cortex and dorsal caudate of the MCA territory. The number of LC3/TUNEL double-positive cells significantly decreased in the HGF ($P < 0.05$)- and GDNF ($P < 0.01$)-treated groups: $238 \pm 49.2/\text{mm}^2$ in vehicle-treated group, $142.8 \pm 38.4/\text{mm}^2$ in HGF-treated group, $71.4 \pm 25.2/\text{mm}^2$ in GDNF-treated group (mean \pm SD; Fig. 6a-c).

DISCUSSION

It was reported that GDNF signals via multicomponent receptors consisting of the Ret receptor tyrosine kinase plus a glycosylphosphatidylinositol-linked coreceptor termed *GDNF family receptor α1* (GFRα1). After binding to its specific receptor complex, GDNF activates several downstream intracellular pathways, including phosphatidylinositol 3-kinase/protein kinase B (PI3K/Akt; Soler et al., 1999) and extracellular signal-regulated kinase 1/2/mitogen-activated protein kinase (ERK1/2 MAPK) pathways (Worby et al., 1996). Signals through PI3K/Akt or ERK1/2MAPK pathways lead to different

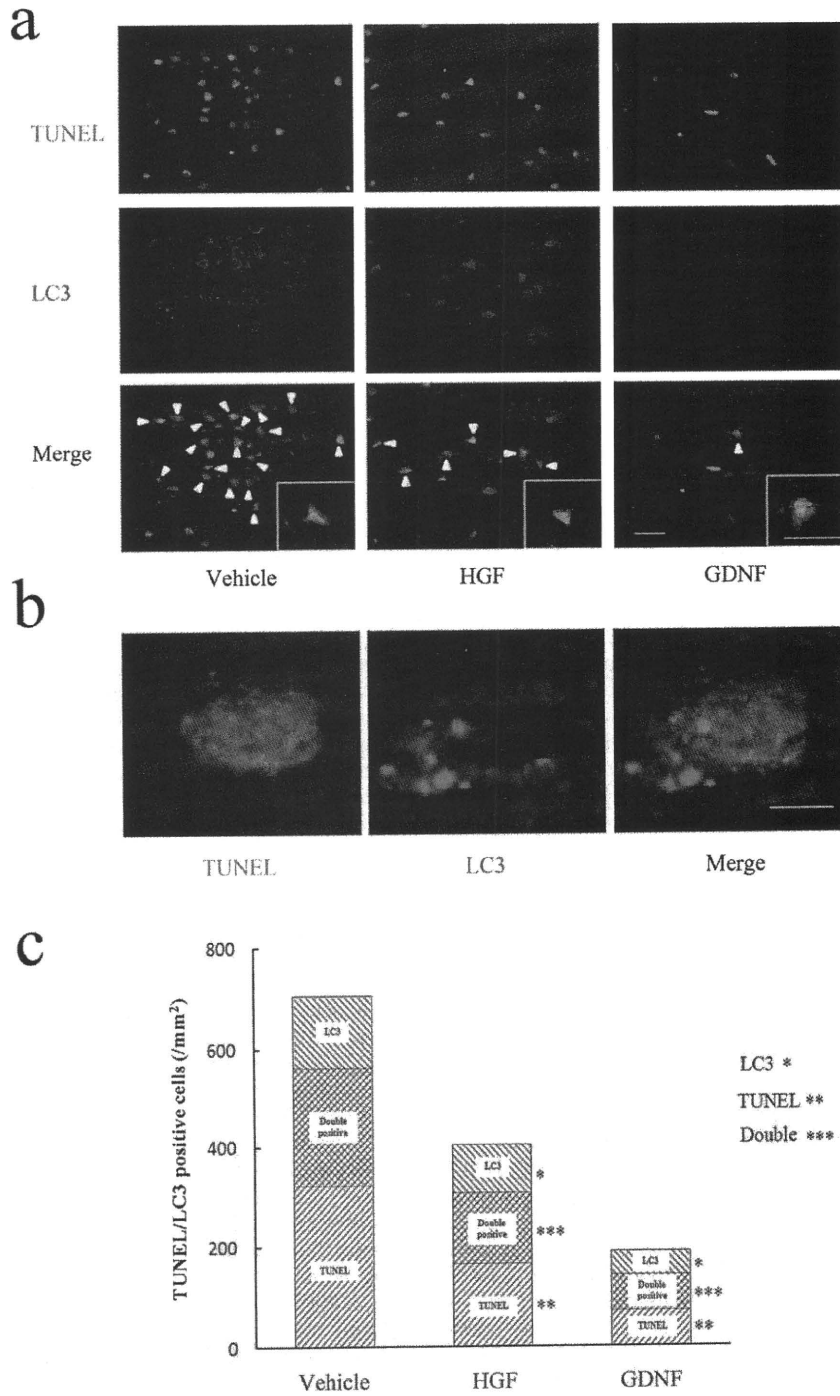


Fig. 6. Photomicrographs of LC3/TUNEL double staining (a,b) and quantitative analysis of LC3/TUNEL double-positive cells (c). The numbers of LC3/TUNEL double-positive cells significantly decreased in the HGF ($P < 0.05$)- and GDNF ($P < 0.01$)-treated groups. * $P < 0.05$ for LC3 vs. vehicle, ** $P < 0.05$ for TUNEL vs. vehicle, *** $P < 0.05$ for double vs. vehicle. Scale bars = 50 μ m in a; 20 μ m in insets; 10 μ m in b.

trophic effects. The most widespread paradigm is that the PI3K/Akt pathway is involved in the cellular survival (Hetman et al., 1999; Vaillant et al., 1999), whereas the ERK1/2 MAPK pathway is involved in neuronal differentiation (Perron et al., 1999). HGF activates the protooncogenic receptor tyrosine kinase c-MET and subsequent downstream pathways, including the antiapoptotic protein kinase-B (PKB/Akt) cascade, the proliferative MAP-kinase pathway (ERK1/2 and p38MAPK), and the STAT3 signaling (signal transducers and activators of transcription; Birchmeier et al., 2003; Okano et al., 2003; Hanada et al., 2004). Similarly, activation of the PI3 kinase/Akt pathway, which is a well known way to inhibit apoptosis, also inhibits autophagy (Arico et al., 2001). Thus, perhaps GDNF and HGF significantly reduced infarct size associated with both the antiapoptotic and the antiautophagic effects (Fig. 1).

From the results of TUNEL staining (Fig. 2), GDNF and HGF had significant antiapoptotic effects. Autophagy was first described in the 1960s (Stromhaug and Klionsky, 2001; Kundu and Thompson, 2008), but many questions about the actual processes and mechanisms involved remain to be elucidated. In multicellular organisms, autophagy is a homeostatic mechanism that may represent the first stage in a cellular/tissue response that can range from autophagy to apoptosis and necrosis (Klionsky and Emr, 2000). In this sense, autophagy is a protective mechanism that can eliminate cells that would otherwise prove harmful to the organism. In fact, autophagy has been suggested to play a critical role in type II (nonapoptotic) programmed cell death (Klionsky and Emr, 2000). To show whether the protective effects of GDNF and HGF are associated with the antiautophagic effect after cerebral ischemia, we examined the protein level of LC3 in ischemic and normal brains. LC3 is associated with autophagosome membranes after post-translational modifications. A C-terminal fragment of LC3 is cleaved immediately after synthesis to yield a cytosolic form called LC3-I (18 kDa). A subpopulation of LC3-I is further converted to an autophagosome-associating form, LC3-II (16 kDa). It was reported that the amount of LC3-II was correlated with the extent of autophagosome formation (Kabeya et al., 2000, 2004). The conversion of LC3-I into LC3-II is accepted as a simple method for monitoring autophagy (Mizushima, 2004; Klionsky et al., 2007). We probed brain sections with an LC3 antibody that detects both forms of LC3, and strong LC3-immunopositive puncta were observed in ischemic brains (Fig. 3a,b). LC3 can under some conditions be incorporated into protein aggregates (Kuma et al., 2007). This is in accordance with Rami et al. (2008), and we found that LC3 is expressed mainly in neurons in the cerebral cortex and dorsal caudate of the MCA territory (Fig. 3c,d).

Western blot analysis of LC3 was performed in our study as well, and we detected that the amount of LC3-I plus LC3-II was significantly higher after cerebral ischemia and that the amount of LC3-II change was crucial in that (Fig. 4). The number of LC3-positive cells

or the amount of LC3 was significantly decreased with GDNF and HGF treatments.

Mammalian target of rapamycin (mTOR) is a phosphatidyl inositol kinase-related kinase that negatively regulates autophagy (Schmelzle and Hall, 2000; Yoritomo and Klionsky, 2005). It has been reported that mTOR function is activated by phosphorylation of Ser²⁴⁴⁸ (Nave et al., 1999; Ravikumar et al., 2003). Recent studies have presented evidence that insulin signal stimulates phosphorylation and activity of mTOR via Akt/PKB signaling (Schmelzle and Hall, 2000). In our study, we confirmed that the level of p-mTOR, an activated form, increased in the HGF and GDNF treated groups (Fig. 5). It can also be hypothesized that GDNF and HGF partially regulated autophagy by the mTOR intracellular signaling pathway. The results described above suggested that both GDNF and HGF have significant antiautophagic effects. Our study suggests that the protective effects of GDNF and HGF were greatly associated both with antiapoptotic and with antiautophagic effects in terms of reducing the number of TUNEL-positive cells, LC3, and activating mTOR. The number of LC3/TUNEL double-positive cells was about 34.3% of LC3 plus TUNEL-positive cells after cerebral ischemia (Fig. 6), which suggested that perhaps one cell can undergo apoptotic cell death or autophagic cell death or two types of cell death at the same time. Thus, it is possible that there are relations between apoptosis and autophagy. It was reported that apoptosis regulator also interacts physically with an autophagy regulator; for example, Beclin 1 can prevent autophagy induction. Beclin 1 was identified as a Bcl-2 interacting protein (Liang et al., 1999), and Beclin 1 also interacts with the other major antiapoptotic Bcl family protein (Bcl-xL) and increases autophagy in nutrient-deprived or growth-factor-withdrawn cells, allowing cell survival (Boya et al., 2005; Lum et al., 2005) by inhibiting apoptosis. In this regard, perhaps in the future GDNF and HGF will be used in cerebral ischemia to protect against neuronal damage. We propose that both GDNF and HGF could provide important therapeutic benefits in terms of not only antiapoptotic but also antiautophagic effects for acute stroke patients. However, when gelfoam is chosen for the delivery of these factors, the amounts of GDNF and HGF should be carefully redetermined before clinical use of these proteins, because better neuroprotective effects in cerebral ischemia have been proved when these proteins are applied intrastrially or intraventricularly using an osmotic pump (Miyazawa et al., 1998; Tsuzuki et al., 2000). Differential roles of GDNF and HGF in chronic cerebral ischemia are of great interests and are currently under investigation in terms of the presence of various extraneurotrophic activities of HGF (Funakoshi and Nakamura, 2003).

ACKNOWLEDGMENTS

We thank Kringle Pharma (Osaka, Japan) for the gift of HGF. The authors declare that they have no competing financial interests.

REFERENCES

- Abe K, Kawagoe J, Araki T, Aoki M, Kogure K. 1992. Differential expression of heat shock protein 70 gene between the cortex and caudate after transient focal cerebral ischemia in rats. *Neurol Res* 14:381-385.
- Abe K, Hayashi T, Itoyama Y. 1997. Amelioration of brain edema by topical application of glial cell line-derived neurotrophic factor in reper-fused rat brain. *Neurosci Lett* 231:37-40.
- Adhami F, Liao G, Morozov YM, Schloemer A, Schmithorst VJ, Lorenz JN, Dunn RS, Vorhees CV, Wills-Karp M, Degen JL, Davis RJ, Mizushima N, Rakic P, Dardzinski BJ, Holland SK, Sharp FR, Kuan CY. 2006. Cerebral ischemia-hypoxia induces intravascular coagulation and autophagy. *Am J Pathol* 169:566-583.
- Arico S, Petiot A, Bauvy C. 2001. The tumor suppressor PTEN positively regulates macroautophagy by inhibiting the phosphatidylinositol 3-kinase/protein kinase B pathway. *J Biol Chem* 276:35243-35246.
- Augustin HG, Braun K, Telemenakis I, Modlich U, Kuhn W. 1995. Ovarian angiogenesis. Phenotypic characterization of endothelial cells in a physiological model of blood vessel growth and regression. *Am J Pathol* 147:339-351.
- Beck KD, Valverde J, Alexi T, Poulsen K, Moffat B, Vandlen RA, Rosenthal A, Hefti F. 1995. Mesencephalic dopaminergic neurons protected by GDNF from axotomy-induced degeneration in the adult brain. *Nature* 373:339-341.
- Birchmeier C, Birchmeier W, Gherardi E, Vande Woude GF. 2003. Met, metastasis, motility and more. *Nat Rev Mol Cell Biol* 4:915-925.
- Bottaro DP, Rubin JS, Falerto DL, Chan AM, Kmiecik TE, Vande Woude GF, Aaronson SA. 1991. Identification of the hepatocyte growth factor receptor as the c-Met proto-oncogene product. *Science* 251:802-804.
- Boya P, Gonzalez-Polo RA, Casares N. 2005. Inhibition of macroautophagy triggers apoptosis. *Mol Cell Biol* 25:1025-1040.
- Cotran RS, Kumar V, Collins T. 1998. Cell injury and cellular death. In: Cotran RS, Kumar V, Collins T, editors. *Robbins pathologic basis of disease*, 6th ed. Philadelphia: Lippincott. p1-29.
- Feig C, Peter ME. 2007. How apoptosis got the immune system in shape. *Eur J Immunol* 37(Suppl 1):S61-S70.
- Funakoshi H, Nakamura T. 2003. Hepatocyte growth factor: from diagnosis to clinical applications. *Clin Chim Acta* 327:1-23.
- Galluzzi L. 2007. Cell death modalities: classification and pathophysiological implications. *Cell Death Differ* 14:1237-1243.
- Green D, Kroemer G. 1998. The central executioner of apoptosis: mitochondria or caspases? *Trends Cell Biol* 8:267-271.
- Hanada M, Feng J, Hemmings BA. 2004. Structure, regulation and function of PKB/AKT—a major therapeutic target. *Biochim Biophys Acta* 1697:3-16.
- Henderson CE, Phillips HS, Pollock RA, Davies AM, Lemeulle C, Annamini M, Simpson LC, Moffet B, Vandlen RA, Koliatsos VE, Rosenthal A. 1997. GDNF: a potent survival factor for motoneurons present in peripheral nerve and muscle. *Science* 266:1062-1064.
- Hetman M, Kanning K, Cavanaugh JE, Xia ZG. 1999. Neuroprotection by brain-derived neurotrophic factor is mediated by extracellular signal-regulated kinase and phosphatidylinositol 3-kinase. *J Biol Chem* 274:22569-22580.
- Honda S, Kagoshima M, Wanaka A, Tohyama M, Matsumoto K, Nakamura T. 1995. Localization and functional coupling of HGF and c-Met/HGF receptor in rat brain: implication as neurotrophic factor. *Brain Res Mol Brain Res* 32:197-210.
- Inbal B, Bialik S, Sabanay I, Shani G, Kimchi A. 2002. DAP kinase and DRP-1 mediate membrane blebbing and the formation of autophagic vesicles during programmed cell death. *J Cell Biol* 157:455-468.
- Kabeya Y, Mizushima N, Ueno T, Yamamoto A, Kirisako T, Noda T, Kominami E, Ohsumi Y, Yoshimori T. 2000. LC3, a mammalian homologue of yeast Apg8p, is localized in autophagosome membranes after processing. *EMBO J* 19:5720-5728.
- Kabeya Y, Mizushima N, Yamamoto A, Oshitani-Okamoto S, Ohsumi Y, Yoshimori T. 2004. LC3, GABARAP and GATE16 localize to autophagosomal membrane depending on form-II formation. *J Cell Sci* 117:2805-2812.
- Kerr JF, Wyllie AH, Currie AR. 1972. Apoptosis: a basic biological phenomenon with wide-ranging implications in tissue kinetics. *Br J Cancer* 26:239-257.
- Kirisako T, Baba M, Ishihara N, Miyazawa K, Ohsumi M, Yoshimori T, Noda T, Ohsumi Y. 1999. Formation process of autophagosome is traced with Apg8/Aut7p in yeast. *J Cell Biol* 147:435-446.
- Kitagawa H, Hayashi T, Mitsumoto Y, Koga N, Itoyama Y, Abe K. 1998. Reduction of ischemic brain injury by topical application of glial cell line-derived neurotrophic factor after permanent middle cerebral artery occlusion in rats. *Stroke* 29:1417-1422.
- Klionsky DJ, Emr SD. 2000. Autophagy as a regulated pathway of cellular degradation. *Science* 290:1717-1721.
- Klionsky DJ, Cregg JM, Dunn WA, Emr SD, Sakai Y, Sandoval IV, Sibirny S, Subramani S, Thumm M, Veenhuis M, Ohsumi Y. 2003. A unified nomenclature for yeast autophagy-related genes. *Dev Cell* 5: 539-545.
- Klionsky DJ, Cuervo AM, Seglen PO. 2007. Methods for monitoring autophagy from yeast to human. *Autophagy* 3:181-206.
- Koizumi J, Yoshida Y, Nakazawa T, Ooneda G. 1986. Experimental studies of ischemic brain edema: A new experimental model of cerebral embolism in rats in which recirculation can be induced in the ischemic area. *Jpn J Stroke* 8:1-7.
- Kroemer G. 2005. Classification of cell death: recommendations of the Nomenclature Committee on Cell Death. *Cell Death Differ* 12(Suppl 2):1463-1467.
- Kuma A, Matsui M, Mizushima N. 2007. LC3, an autophagosome marker, can be incorporated into protein aggregates independent of autophagy. *Autophagy* 3:328-332.
- Kundu M, Thompson CB. 2008. Autophagy: basic principles and relevance to disease. *Annu Rev Pathol* 3:427-455.
- Liang XH, Jackson S, Seaman M. 1999. Induction of autophagy and inhibition of tumorigenesis by beclin 1. *Nature* 402:672-676.
- Lin L-FH, Doherty DH, Lile JD, Bektesh S, Collins F. 1993. GDNF: a glial cell line-derived neurotrophic factor for midbrain dopaminergic neurons. *Science* 260:1130-1132.
- Lin L, Wu W, Lin LF, Lei M, Oppenheim RW, Houenou LJ. 1995. Rescue of adult mouse motoneurons from injury-induced cell death by glial cell line-derived neurotrophic factor. *Proc Natl Acad Sci U S A* 92:9771-9775.
- Lum JJ, Bauer DE, Kong M. 2005. Growth factor regulation of autophagy and cell survival in the absence of apoptosis. *Cell* 120:237-248.
- Maina F, Klein R. 1999. Hepatocyte growth factor, a versatile signal for developing neurons. *Nat Neurosci* 2:213-217.
- Maina F, Hilton MC, Andres R, Wyatt S, Klein R, Davies AM. 1998. Multiple roles for hepatocyte growth factor in sympathetic neuron development. *Neuron* 20:835-846.
- Matsumoto K, Nakamura T. 1996. Emerging multipotent aspects of hepatocyte growth factor. *J Biochem* 119:591-600.
- Matsumoto K, Nakamura T. 1997. Hepatocyte growth factor (HGF) as a tissue organizer for organogenesis and regeneration. *Biochem Biophys Res Commun* 239:639-644.
- Miyazawa T, Matsumoto K, Ohmichi H, Katoh H, Yamashita T, Nakamura T. 1998. Protection of hippocampal neurons from ischemia-induced delayed neuronal death by hepatocyte growth factor: a novel neurotrophic factor. *J Cereb Blood Flow Metab* 18:345-348.
- Mizushima N. 2004. Methods for monitoring autophagy. *Int J Biochem Cell Biol* 36:2491-2502.

- Nagasawa H, Kogure K. 1989. Correlation between cerebral blood flow and histologic changes in a new rat model of middle cerebral artery occlusion. *Stroke* 20:1037-1043.
- Nakamura T, Nawa K, Ichihara A. 1984. Partial purification and characterization of hepatocyte growth factor from serum of hepatectomized rats. *Biochem Biophys Res Commun* 122:1450-1459.
- Nakamura T, Nishizawa T, Hagiya M, Seki T, Shimonishi M, Sugimura A, Tashiro K, Shimizu S. 1989. Molecular cloning and expression of human hepatocyte growth factor. *Nature* 342:440-443.
- Nave BT, Ouwens M, Withers DJ, Alessi DR, Shepherd PR. 1999. Mammalian target of rapamycin is a direct target for protein kinase B: identification of a convergence point for opposing effects of insulin and amino-acid deficiency on protein translation. *Biochem J* 344:427-431.
- Niimura M, Takagi N, Takagi K, Funakoshi H, Nakamura T, Takeo S. 2006a. Effects of hepatocyte growth factor on phosphorylation of extracellular signal-regulated kinase and hippocampal cell death in rats with transient forebrain ischemia. *Eur J Pharmacol* 27:114-124.
- Niimura M, Takagi N, Takagi K, Mizutani R, Ishihara N, Matsumoto K, Funakoshi H, Nakamura T, Takeo S. 2006b. Prevention of apoptosis-inducing factor translocation is a possible mechanism for protective effects of hepatocyte growth factor against neuronal cell death in the hippocampus after transient forebrain ischemia. *J Cereb Blood Flow Metab* 26:1354-1365.
- Okano J, Shiota G, Matsumoto K, Yasui S, Kurimasa A, Hisatome I, Steinberg P, Murawaki Y. 2003. Hepatocyte growth factor exerts a proliferative effect on oval cells through the PI3K/AKT signaling pathway. *Biochem Biophys Res Commun* 309:298-304.
- Otto D, Frotscher M, Uniscker K. 1989. Basic fibroblast growth factor and nerve growth factor administered in gel foam rescue medial septal neurons after fimbria fornix transection. *J Neurosci Res* 22:83-91.
- Perron JC, Bixby JL. 1999. Distinct neurite outgrowth signaling pathways converge on ERK activation. *Mol Cell Neurosci* 13:362-378.
- Rami A, Langhagen A, Steiger S. 2008. Focal cerebral ischemia induces up-regulation of Beclin 1 and autophagy-like cell death. *Neurobiol Dis* 29:132-141.
- Ravikumar B, Stewart A, Kita H, Kato K, Duden R, Rubinsztein DC. 2003. Raised intracellular glucose concentrations reduce aggregation and cell death caused by mutant huntingtin exon 1 by decreasing mTOR phosphorylation and inducing autophagy. *Hum Mol Genet* 12:985-994.
- Reggiori F, Klionsky DJ. 2002. Autophagy in the eukaryotic cell. *Eukaryot. Cell* 1:11-21.
- Russell WE, McGowan JA, Bucher NL. 1984. Partial characterization of a hepatocyte growth factor from rat platelets. *J Cell Physiol* 119:183-192.
- Schmelzle T, Hall MN. 2000. TOR, a central controller of cell growth. *Cell* 103:253-262.
- Soler RM, Dolcet X, Encinas M, Egea J, Bayascas JR, Comella JX. 1999. Receptors of the glial cell line-derived neurotrophic factor family of neurotrophic factors signal cell survival through the phosphatidylinositol 3-kinase pathway in spinal cord motoneurons. *J Neurosci* 19:9160-9169.
- Stromhaug PE, Klionsky DJ. 2001. Approaching the molecular mechanism of autophagy. *Traffic* 2:524-531.
- Sun W, Funakoshi H, Nakamura T. 2002. Overexpression of HGF retards disease progression and prolongs life span in a transgenic mouse model of ALS. *J Neurosci* 22:6537-6548.
- Tomac A, Lindqvist E, Lin LF, Gren SO, Young D, Hoffer BJ, Olson L. 1995. Protection and repair of the nigrostriatal dopaminergic system by GDNF in vivo. *Nature* 373:335-339.
- Tsuzuki N, Miyazawa T, Matsumoto K, Nakamura T, Shima K, Chigasaki H. 2000. Hepatocyte growth factor reduces infarct volume after transient focal cerebral ischemia in rats. *Acta Neurochir Suppl* 76:311-316.
- Tsuzuki N, Miyazawa T, Matsumoto K, Nakamura T, Shima K. 2001. Hepatocyte growth factor reduces the infarct volume after transient focal cerebral ischemia in rats. *Neurol Res* 23:417-424.
- Vaillant AR, Mazzoni I, Tudan C, Boudreau M, Kaplan DR, Miller FD. 1999. Depolarization and neurotrophins converge on the phosphatidylinositol 3-kinase-Akt pathway to synergistically regulate neuronal survival. *J Cell Biol* 146:955-966.
- Van Belle E, Witzenbichler B, Chen D, Silver M, Chang L, Schwall R, Isner JM. 1998. Potentiated angiogenic effect of scatter factor/hepatocyte growth factor via induction of vascular endothelial growth factor: the case for paracrine amplification of angiogenesis. *Circulation* 97:381-390.
- Wang Y, Lin SZ, Chiou AL, Williams LR, Hoffer BJ. 1997. Glial cell line-derived neurotrophic factor protects against ischemia-induced injury in the cerebral cortex. *J Neurosci* 17:4341-4348.
- Worby CA, Vega QC, Zhao Y, Chao HH, Seasholtz AF, Dixon JE. 1996. Glial cell line-derived neurotrophic factor signals through the RET receptor and activates mitogen-activated protein kinase. *J Biol Chem* 271:23619-23622.
- Yorimitsu T, Klionsky DJ. 2005. Autophagy: molecular machinery for self-eating. *Cell Death Differ* 12(Suppl 2):1542-1552.
- Yoshimori T. 2004. Autophagy: a regulated bulk degradation process inside cells. *Biochem Biophys Res Commun* 313:453-458.
- Zarnegar R, Michalopoulos GK. 1995. The many faces of hepatocyte growth factor: from hepatopoiesis to hematopoiesis. *J Cell Biol* 129:1177-1180.
- Zhao MZ, Nonoguchi N, Ikeda N, Watanabe T, Furutama D, Miyazawa D, Funakoshi H, Kajimoto Y, Nakamura T, Dezawa M, Shibata MA, Otsuki Y, Coffin RS, Liu WD, Kuroiwa T, Miyatake S. 2006. Novel therapeutic strategy for stroke in rats by bone marrow stromal cells and ex vivo HGF gene transfer with HSV-1 vector. *J Cereb Blood Flow Metab* 26:1176-1188.

ALSに対するヒト型組み換えHGF蛋白を用いた第1相試験(治験)

東北大学大学院医学系研究科 神経内科 東北大学病院 ALS治療開発センター *現、国立精神・神経医療研究センター病院
青木正志・割田 仁・糸山泰人*

1. はじめに

筋萎縮性側索硬化症(ALS)は運動をつかさどる神経(運動ニューロン)だけが傷害を受けることにより、全身の筋肉がやせて力が入らなくなり、やがて呼吸不全にいたるという最も厳しい神経難病です。ALSはこれまでは全く原因不明とされてきましたが、家族内でこのALSを発症する家系(家族性ALS)の一部が銅、亜鉛スーパーオキシドジスムターゼ(Cu/Zn SODあるいはSOD1)遺伝子異常により起こることが、1993年に米国ボストンのハーバード大学を中心とするグループにより発見されました。この時点で、ALSはもはや“原因不明の病気”ではなくなったのです。これまでに、日本をふくめた世界中の患者さんからSOD1遺伝子の異常が報告されています¹⁾。その後の研究の進展で、TDP-

43、FUSなどの新しい原因遺伝子による家族性ALSが報告されています。さらに本年の5月には広島大学の川上秀史先生らはoptineurinが新たな原因遺伝子であることを発見しています²⁾。一方、9割以上のALS患者さんは家族性でなく、その患者さんだけが病気を発症し、孤発性ALSと呼ばれますが、この孤発性ALSの病態の解明も進んでいます。

ヒトの病気と同じ症状を示す動物を疾患モデル動物と呼びますが、モデル動物はヒトの病気の病態解明・治療研究を行うのにとっても重要な役割を果たしてきました。これまでもいくつかのALSのモデル動物が知られていましたが、最近の遺伝子工学の技術革新はめざましく、遺伝子解析により発見された患者さんの遺伝子異常をそのままマウスに導入して、マウスに同じような病気を作らせることが可能

になりました。このマウスではヒトのALSと同じように脊髄にある運動ニューロンが病気の進行と共に萎縮して脱落しています。このように、ある特定の遺伝子を人工的に導入したマウスをトランスジェニックマウスと呼んでいます。ALSの場合でも、実際に患者さんにみられたSOD1遺伝子異常をマウスに導入し、トランスジェニックマウスを作ることによりヒトの病気に近いモデルマウスが作製されています。さらには、新しい薬を患者さんに投与する前にこのトランスジェニックマウスに投与し、その効果を検討することも行われています。実際に現在ALSに対して唯一認可された治療薬であるリルゾール(リルテック[®])もトランスジェニックマウスに投与され、病気の進行を遅らせることが明らかになっています。

2. HGFによる治療法の開発

肝細胞増殖因子(HGF)はわが国の中村敏一先生らによって発見された新しい増殖因子です。HGFは文字通り肝臓で発見されましたが、その後の研究で、神経細胞に対しても神経栄養因子として働くこ

とが明らかになり、なかでも運動ニューロンに対して非常に強力な再生誘導因子として働くことが明らかになりました。さらに大阪大学の船越 洋先生はHGFを遺伝子工学的にALSマウス導入することによりALSの進行を抑制することを示し³⁾、ALSの新しい治療薬として注目されています。

ALSに対する治療法の開発のために、東北大学神経内科ではトランスジェニックラットによるALSモデル動物(ALSラット)の開発に成功しました⁴⁾。このALSラットを利用しHGFを効率的に脊髄の運動ニューロンに到達させるために、浸透圧ポンプを用いてヒト型組み換えHGF蛋白の脊髄腔内への持続投与を行ないました(図1、右上)。その結果、発症期からのHGF投与を開始により病気の進行を抑えることが確認されました⁵⁾。図1の実線はHGF投与群、点線は対照群(HGFを使用していないグループ)の経過を示しています。病気の発症から死亡までの罹病期間が、HGF投与群が 27.5 ± 11.1 日間、対照群が 16.9 ± 8.17 日間と、HGF投与群では対照群の62.7%の増大を示しています。HGFがALSラットの罹病期間を大幅に延長させ、ALSの進行を遅ら

せることがわかりました。

平成20年11月から内閣府を中心とした国家プロジェクトとして新薬開発のための先端医療開発特区(スーパー特区)制度が始まりましたが、HGFはわが国発のALS治療薬候補としてそのスーパー特区に選定され(代表は岡野栄之 慶應義塾大学医学部生理学教授)、その中での最先導課題となっています。

3. 治験とは

新しい薬が一般に使われるようになるためには、効果がありそうな「新しい薬の候補」について動物による試験を行います(非臨床試験といいます)。そこで十分に検討された後、少数の健康な成人の方実際に服用していただき、新しい薬の候補の安全

性を検討します。次に実際に患者さんに服用していただき、「その新しい薬の候補が病気に対してどれだけ効くか(効果)」と「どのような種類の副作用がどの位の割合で起こるのか(安全性)」を検討するための試験を行います。このような人に対して行われる臨床試験のうち、特に国(厚生労働省)に医薬品として認めてもらうために行われる試験を「治験」と呼びます。今回のヒト型組み換えHGF蛋白の治験は腰椎穿刺を行なうことによる髄腔内投与を行なうため、第一相試験にも患者さんの協力を得て行なうことを検討しています。

「治験」は薬事法や国が定めたルールに従って行われ、これらの結果を厚生労働省が審査した後、薬として承認されれば他の患者さんにも広く使ってもらえるようになります。今、病院で使用

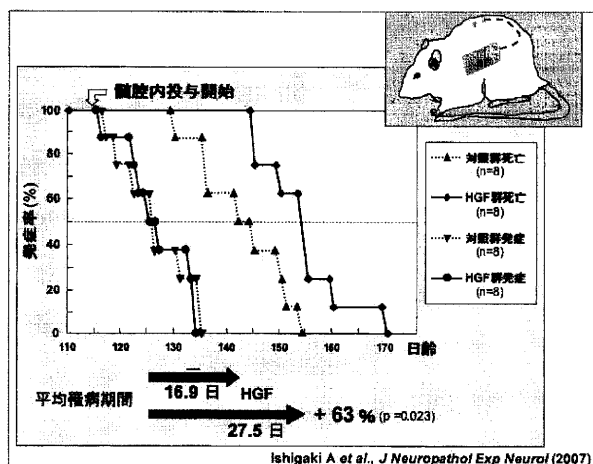


図1 HGF投与によるALS進行抑制効果

実線はHGF投与群、点線は対照群(HGFを使用していないグループ)の経過を示しています。発症期の投与になりますので、両群での発症は差を認めません。一方で平均死亡(この実験の場合はラットが自分で起き上がれず、えさが食べられない状態を死亡と定義しています)はHGF投与群が154.3±16.4日、対照群が143.25±17.0日とHGF投与群が対照群より大幅に遅れています。病気の発症から死亡までの罹病期間が、HGF投与群が27.5±11.1日間、対照群が16.9±8.17日間と、HGF投与群では対照群の62.7%の増大を示しており、発症期からの投与によってもHGFがALSラットの罹病期間を延長させ、ALS病態の進行を大幅に遅らせることができました。

されている薬も、先人の協力によって「治験」という段階を経て厚生労働省の承認が得られました。治験は参加される患者さんが不利益を受けないよう、病院の治験審査委員会(治験について審査する委員会)により十分検討され、実施を承認したものが実施されます。

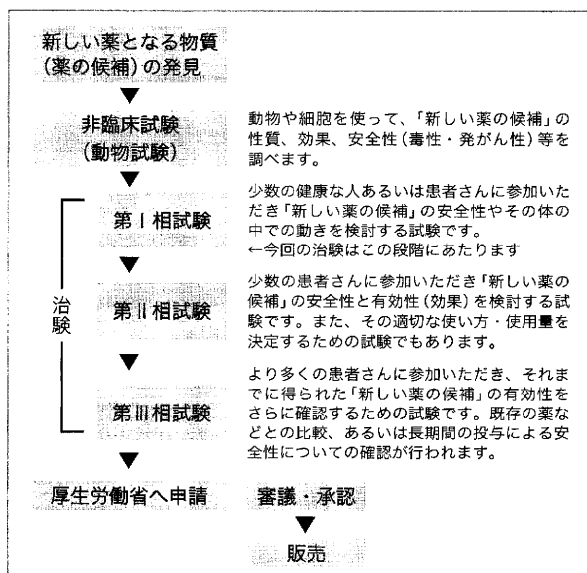


図2 治験の一般的な進め方

4. 現在の進行状況

東北大学病院ではヒト型組み換えHGF蛋白を用いたALSの治療法の開発を進めています。私たちはHGFを効率的に脊髄の運動ニューロンに到達させるために腰椎穿刺により脊髄腔内へ投与することを計画しています。これまでに、ヒトに対する治験を開始するために必要な動物を用いた試験(非臨床試験)であるHGFを脊髄腔内へ投与した時の安全性試験および薬物動態試験が終了しました。この結果に基づき、現在、治験を行うための実施計画書(プロトコル)を作成中です(図3)。

治験にはいくつかの段階が必要となります。まずは第1相試験で、HGFを脊髄腔内へ投与した時の安全性および薬物動態(どのくらいの間、髄腔内へとどまるかなど)を確かめる必要があります、この第1

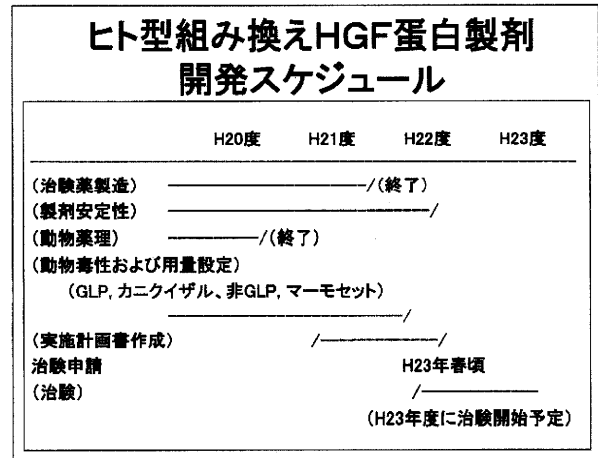


図3 ヒト組み換えHGF蛋白質製剤の開発スケジュール
カニクイザルに対してGLP基準(Good Laboratory Practice薬事法によるデータの信頼性を確保するための実施基準)に従ったヒト型リコンビナントHGF蛋白髄腔内持続投与の安全性試験(赤字)は終了し、現在、治験届けを提出するために実施計画書を作成中です。

相試験の開始を平成23年4月を目標に、日夜、準備を進めています。

現在、東北大学病院と製薬会社が一緒に治験に参加していただく患者さんの条件、期間、などを検討中の段階であり、厚生労働省(医薬品医療機器総合機構)とも相談中です。従って、未だ皆様へ治験の正式な開始時期、詳細などをお伝えすることはできません。患者さんの登録も行なっておりません。今後、厚生労働省へ正式に治験届けを提出し、厚生労働省から実施計画書などの調査を受け、治験を実施することに問題がないと判断された後に、皆様へご連絡させていただくことになります。この連絡は日本ALS協会を通じても行いたいと考えております。

5. 最後に

製薬会社が参入しがたい分野は大学をはじめとする研究機関が中心となって治療法の開発を進めるしか道はありません。わが国には基礎研究の成果がたくさんあります。しかし残念なことにそれを治療薬として開発していく手段があまりにも貧弱です。基礎研究の成果を医療として実用化する研究を橋渡し

研究あるいはトランスレーショナルリサーチと呼んでいますが、このトランスレーショナルリサーチを動かして行かないと、ALSの治療法の開発は進みません。スーパー特区制度などを大いに利用してALSの治療法の開発を進めたいと思います。

■文献

- 1) Aoki M, Ogasawara M, Matsubara Y et al: Mild ALS in Japan associated with novel SOD mutation [published erratum appears in Nature Genet. 6: 225, 1994]. Nature Genet 1993; 5: 323-4.
- 2) Maruyama H, Morino H, Ito H et al., Mutations of optineurin in amyotrophic lateral sclerosis. Nature 2010; 465:223-6
- 3) Sun W, Funakoshi H, Nakamura T, Overexpression of HGF retards disease progression and prolongs life span in a transgenic mouse model of ALS. J Neurosci 2002; 22: 6537-48.
- 4) Nagai M, Aoki M, Miyoshi I et al., Rats expressing human cytosolic copper-zinc superoxide dismutase transgenes with amyotrophic lateral sclerosis: associated mutations develop motor neuron disease. J Neurosci 2001; 21: 9246-54
- 5) Ishigaki A, Aoki M, Nagai M et al., Intrathecal delivery of HGF from the ALS onset suppresses disease progression in a rat ALS model, J Neuropathol Exp Neurol, 2007; 66: 1037-44

日本臨牀 68巻 増刊号7 (2010年7月20日発行) 別刷

広範囲 血液・尿化学検査 免疫学的検査

—その数値をどう読むか—

[第7版]

(4)

X. プロスタノイド, サイトカイン, 増殖因子, ケモカイン

肝細胞増殖因子(HGF)

野間さつき 船越 洋 中村敏一

肝細胞増殖因子(HGF)

HGF levels in serum, cerebrospinal fluid, joint fluid,
tissues and various diseases

野間さつき¹ 船越 洋¹ 中村敏一²

Key words : c-Met, 血清, 脳脊髄液, 癌, 関節液

1. 概 説

肝細胞増殖因子(hepatocyte growth factor: HGF)は1984年, 中村らにより肝再生中のラットの血清より部分精製され¹⁾, 1989年にヒトHGFがクローニングされた²⁾. その構造は, クリンドメインを4つ含む α 鎖(69kDa)と, セリンプロテアーゼ様構造をもつ β 鎖(34kDa)から

なる. 初め一本鎖のプロ体として産生され, HGF converting enzyme もしくは HGF activator, u-PA(urokinase-type plasminogen activator), t-PA(tissue-type PA), matriptase などにより α 鎖と β 鎖間の Arg-Val 部位で切断され二本鎖 HGF となり初めて c-Met/HGF 受容体と結合し活性化できるようになる(図1-a).

HGFの生物活性は当初の肝細胞増殖活性に

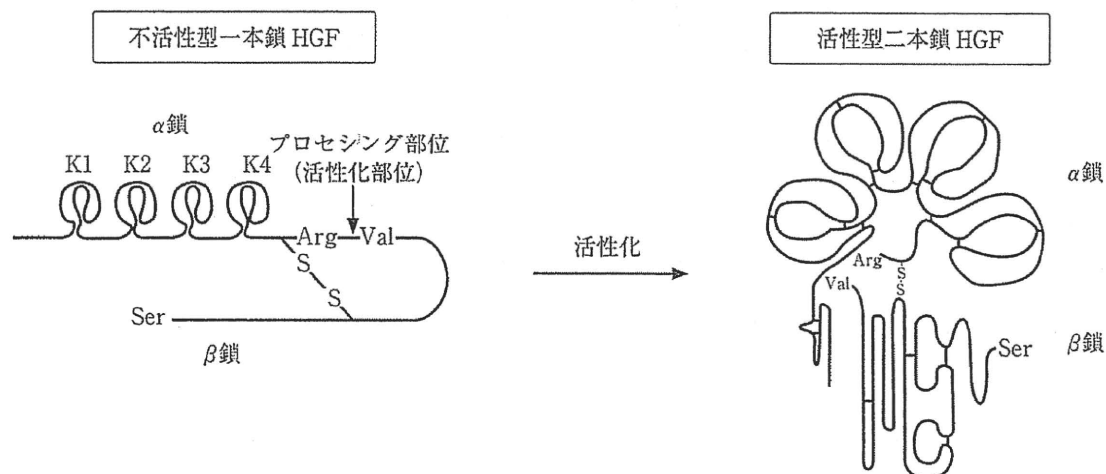


図1-a HGFの構造と傷害組織特異的作用分子機構の模式図
—HGFの構造と活性化機構—

¹Satsuki Noma, Hiroshi Funakoshi: Division of Molecular Regenerative Medicine, Department of Biochemistry and Molecular Biology, Osaka University Graduate School of Medicine/Division of Virology, Department of Microbiology and Immunology, Osaka University Graduate School of Medicine 大阪大学大学院医学系研究科 生化学・分子生物学講座 分子再生医学/大阪大学大学院医学系研究科 感染免疫医学講座 ウイルス学 ²Toshikazu Nakamura: Kringle Pharma Joint Research Division for Regenerative Drug Discovery, Center for Advanced Science and Innovation, Osaka University 大阪大学先端科学イノベーションセンター クリングルファーマ再生創薬共同研究部門